



# Transport Modeling of Interplanetary Electrons in the 2002 October 20 Solar Particle Event

W. Dröge<sup>1</sup> , Y. Y. Kartavykh<sup>1,2</sup> , L. Wang<sup>3</sup> , D. Telloni<sup>4</sup> , and R. Bruno<sup>5</sup>

<sup>1</sup> Institute for Theoretical Physics and Astrophysics, University of Würzburg, Würzburg, Germany

<sup>2</sup> Ioffe Physical-Technical Institute, St. Petersburg 194021, Russia

<sup>3</sup> School of Earth and Space Sciences, Peking University, 100871 Beijing, People's Republic of China

<sup>4</sup> INAF-OATo Osservatorio Astronomico di Torino, Via Osservatorio 20, I-10025 Pino Torinese, Italy

<sup>5</sup> INAF-IAPS Istituto di Astrofisica e Planetologia Spaziali, Via del Fosso del Cavaliere 100, I-00133 Roma, Italy

Received 2018 August 9; revised 2018 September 27; accepted 2018 October 26; published 2018 December 21

## Abstract

We analyze electrons in the energy range 1–180 keV, observed by the *Wind* spacecraft following an impulsive solar flare on 2002 October 20. The event is characterized by weak, but measurable pitch-angle scattering, which allows a characterization of the pitch-angle scattering coefficient  $D_{\mu\mu}(\mu)$ , as well as by particle reflection at an outer boundary. Based on numerical solutions of the focused transport equation we present fits to the observed electron fluxes, with emphasis on a detailed modeling of the particles' angular distributions. By means of the wavelet transform method we estimate the slab component of the fluctuation, which is frequently assumed to dominate the particle scattering. We find that the values of  $D_{\mu\mu}(\mu)$  obtained from the modeling for several energy ranges disagree strongly with the ones calculated from the estimated slab component for this event and standard quasi-linear theory, in the pitch-angle dependence of the scattering coefficient and also in its magnitude. These results indicate that in this event the scattering of electrons at low energies is much weaker than predicted by the above models, and that at large wavenumbers the slab component makes up only a few per cent of the fluctuations. We discuss whether in weak-scattering events the concept of pitch-angle diffusion due to a resonant interaction of the particles with the turbulence would have to be reconsidered, and whether additional effects such magnetic mirroring of the electrons and intermittency of the fluctuations would have to be taken into account.

*Key words:* Sun: heliosphere – Sun: particle emission – turbulence

## 1. Introduction

According to their characteristics, solar energetic particle (SEP) events are typically separated into two classes (e.g., Reames 1999): gradual events, which exhibit particle fluxes lasting for several days, are rather proton-rich, and are associated with interplanetary shock waves, and impulsive events, which are electron-rich, exhibit timescales for the observed fluxes of several hours, and are believed to be associated with flares. Particles in gradual events are considered to be energized mainly at traveling interplanetary shock waves, due to reflection at the shock, shock drift acceleration, or diffusive shock acceleration (e.g., Drury 1983). The gradual increase in particle fluxes is caused by the continuous acceleration at the shock front, and the usually extended shock fronts can lead to broad angular spreads of the accelerated particles. Impulsive SEP events (also called electron/<sup>3</sup>He-rich SEP events), such as the one considered in this work, are dominated by  $\sim 1$ –100 keV electrons (Wang et al. 2012) and low-intensity  $\sim$ MeV/nucleon ion emissions with large enhancements of <sup>3</sup>He (by a factor of up to  $\sim 10^4$  times the coronal values), heavy nuclei such as Fe (by a factor of  $\sim 10$ ), and ultraheavy nuclei up to  $\sim 200$  amu (by a factor of  $> 200$ ), and high ionization states (e.g., Fe<sup>20+</sup>) (see Mason 2007, for review). Particles in impulsive events are considered to be energized in solar flares by stochastic acceleration and/or in a process involving magnetic reconnection. At solar maximum,  $\gtrsim 150$  solar electron events/year are observed near the Earth with a longitude extent of  $\sim 30^\circ$ – $60^\circ$ , implying the occurrence of  $\sim 10^4$  events/year over the whole Sun (Wang et al. 2012).

The timing of particle injection in impulsive SEP events carries important information for understanding the acceleration of electrons and <sup>3</sup>He-rich ions. Krucker et al. (1999) and Haggerty & Roelof (2002) found that the injection of the  $> 25$ –38 keV electrons at the Sun was delayed by  $\sim 10$  to 30 minutes after the release of type-III radio bursts in most ( $\sim 80\%$ ) of impulsive events. Wang et al. (2006) reported that the observed in situ flux–time profiles for three strongly scatter-free electron events fit well to an isosceles triangle injection profile (with equal rise and fall times) at the Sun, with the low-energy ( $\sim 0.4$ –10 keV) electron injection starting  $\sim 9$  minutes before the type-III bursts but the high-energy ( $\sim 10$ –300 keV) electron injection starting  $\sim 8$  minutes after, suggesting that low-energy electrons generate the type-III radio emissions. Moreover, Reames et al. (1985) showed in one electron/<sup>3</sup>He-rich SEP event that <sup>3</sup>He-rich ions were injected close to the electron injection (within  $\sim 1$  hr), while Ho et al. (2003) reported five electron/<sup>3</sup>He-rich events with a delayed ( $> 40$  minutes) ion injection. More recently, Wang et al. (2016) examined the timing of electron and ion injections at the Sun for 10 good electron/<sup>3</sup>He-rich SEP events, using a 1.2 au particle path length. They found that, on average, the injection of low-energy ( $\sim 0.4$  to 9 keV) electrons starts first and lasts for  $\sim 90$  to  $\sim 160$  minutes, the injection of high-energy ( $\sim 10$  to 300 keV) electrons starts  $17 \pm 3$  minutes after the start of the low-energy electron injection and lasts for only  $\sim 10$  to  $\sim 30$  minutes, and the injection of  $\sim 0.1$ –2 MeV/nucleon ions begins  $75 \pm 14$  minutes after the start of the low-energy electron injection, and lasts for  $\sim 200$  to  $\sim 550$  minutes.

Because of their comparatively small gyro radii, electrons with energies of a few keV to a few tens of keV interact

resonantly with magnetic fluctuations in the solar wind that have small wavelengths. The amplitudes of these fluctuations are typically small, as observations of their power spectral densities show (Bruno et al. 2004). Correspondingly, the scattering of low-energy electrons, compared to that of electrons and protons with  $\sim$ MeV energies, is usually rather weak, and their transport is occasionally characterized as “scatter-free” (Lin 1974). As we will demonstrate in this work, the propagation of low-energy electrons cannot be really scatter-free (in which case their pitch angles would be within one degree at 1 au due to adiabatic focusing in the radially decreasing heliospheric magnetic field), but can be weak enough to preserve information, as mentioned above, about their injection close to the Sun, about the nature of their scattering at magnetic fluctuations, and occasionally also about their interaction with reflecting boundaries at distances from the Sun of 2 au and beyond.

In events with strong scattering the observed angular distributions of the particles are usually composed of a large isotropic part and a small anisotropic part, which is roughly proportional to a first-order Legendre polynomial in the cosine of the particle’s pitch angle. The transport of the particles can then be described reasonably well by spatial diffusion and an associated mean free path. By contrast, pitch-angle distributions in events with weak scattering often exhibit a more complicated structure, which can be related to properties of the magnetic fluctuations and the functional form of the pitch-angle diffusion coefficients. These possibilities had been exploited by, e.g., Qin et al. (2005), who modeled *Wind*/STEP observations of the pitch-angle-dependent transport of  $\sim$ 0.5 MeV/nucleon helium and found that the value of the resulting mean free path would depend strongly on the functional form of the pitch-angle diffusion coefficient, and Dröge & Kartavykh (2009), who concluded that pitch-angle distributions of  $\sim$ 100 keV electrons in an event with weak scattering have little resemblance to predictions from quasi-linear theory (QLT) and the standard assumption of a 20% slab/80% two-dimensional composition of the fluctuations. Under weak scattering conditions it is occasionally observed (e.g., Anderson et al. 1995) that a pulse of solar electrons passing a spacecraft in the anti-sunward direction is followed by another pulse after a time span of one hour or so, this time propagating in the sunward direction. Such observations indicate that the second pulse, which might be considerably weaker and broader, consists of electrons from the first pulse that had been reflected, possibly due to mirroring, at a magnetic compression located at a distance of 1–2 au along the magnetic field line beyond the spacecraft. Possible magnetic field structures that could explain the reflection of particles include compressions related to coronal mass ejections (CMEs, Tan et al. 2009) and corotating interaction regions (CIRs, Wang et al. 2011), as well as to the compressed magnetic field behind interplanetary shocks (Tan et al. 2012), or the converging field lines at the far leg of the loop structures associated with magnetic clouds (Saiz et al. 2008). For the 1998 May 2 solar particle event Malandraki et al. (2002) studied angular distributions of energetic electrons observed on *ACE* when the spacecraft was located inside a magnetic cloud, with the solar wind speed being of the order of  $600 \text{ km s}^{-1}$ . They concluded that the electrons propagated without much scattering and were reflected by a magnetic field enhancement in the downstream region of the associated CME-driven shock. For

the same event Torsti et al. (2004) analyzed *Solar and Heliospheric Observatory*/ERNE observations of solar 17–22 MeV protons and found that the protons also propagated almost scatter-free, corresponding to a mean free path of  $\sim$ 10 au, and they also identified a counter-streaming flux commencing 30–45 minutes after the onset of the proton event. The above findings seem to suggest that fast solar wind streams are associated with magnetic fluctuations that scatter energetic particles comparatively weakly, and if a magnetic compression is present down the connecting field line they allow the detection of reflected particle pulses.

The structure of the paper is as follows. In Section 2 we give an overview of electromagnetic emission from the Sun, interplanetary electron fluxes in the energy range from keV to tens of keV, and solar wind parameters observed during a time period comprising the 2002 October 20 solar particle event. In Section 3 we introduce the formalism to describe the pitch-angle-dependent transport of solar particles along the magnetic field in the inner heliosphere, and the relation between the particle’s pitch-angle diffusion coefficient and the power spectral densities of the observed magnetic fluctuations in the solar wind. In Section 4 we present results of the transport modeling of the electrons with a focus on a detailed comparison of the observed pitch-angle distributions with those predicted from the modeling, and on the interaction of the electrons with an outer boundary. In Section 5 we discuss the implications of our results for the validity of certain versions of QLT and assumptions of the geometry of the solar wind fluctuations, and summarize our conclusions.

## 2. Observations and Data Analysis

The solar particle event of 2002 October 20, which was associated with a *GOES* C6.6 flare at approximately S20 and W63, has been widely studied (e.g., Wang et al. 2011) although, to our knowledge, detailed modelings of the particle transport and an analysis of the solar wind turbulence have not been performed so far. Here we analyze *Wind* electron observations made by the 3-Dimensional Plasma and Energetic Particle (3DP) instrument (Lin et al. 1995), magnetic field observations from the MFI instrument (Lepping et al. 1995), and plasma observations from the SWE instrument (Ogilvie et al. 1995). The *Wind* spacecraft was launched on 1994 November 1 with a trajectory consisting mostly of highly elliptical Earth orbits (apogees  $\sim$ 60–100  $R_E$ ) or orbits around the Lagrange 1 point. During the onset of the particle event *Wind* was located in the solar wind at  $X = 99.8$ ,  $Y = 5.9$ , and  $Z = 5.2$  (geocentric solar ecliptic (GSE) coordinates, units of Earth radii). A number of bursts in the ion fluxes below 1 MeV/nucleon (not shown here; see also the magnetic field angles displayed in Figure 1) indicate occasional magnetic connections of *Wind* with the bow shock, but they do not affect the results presented here.

Figure 1 shows the observed electromagnetic emission from the Sun, electron fluxes, and solar wind plasma data during the time of the particle event. The soft X-ray flux (first panel) peaked at 14:00 UT (*GOES* geophysical data website). Radio emission due to electrons streaming away from the Sun was detected by the *Wind*/Waves instrument setting in at 14:15 UT, indicating that accelerated electrons had immediate access to interplanetary space (second panel). The third panel shows omnidirectional fluxes of 0.9–517 keV electrons. Following the

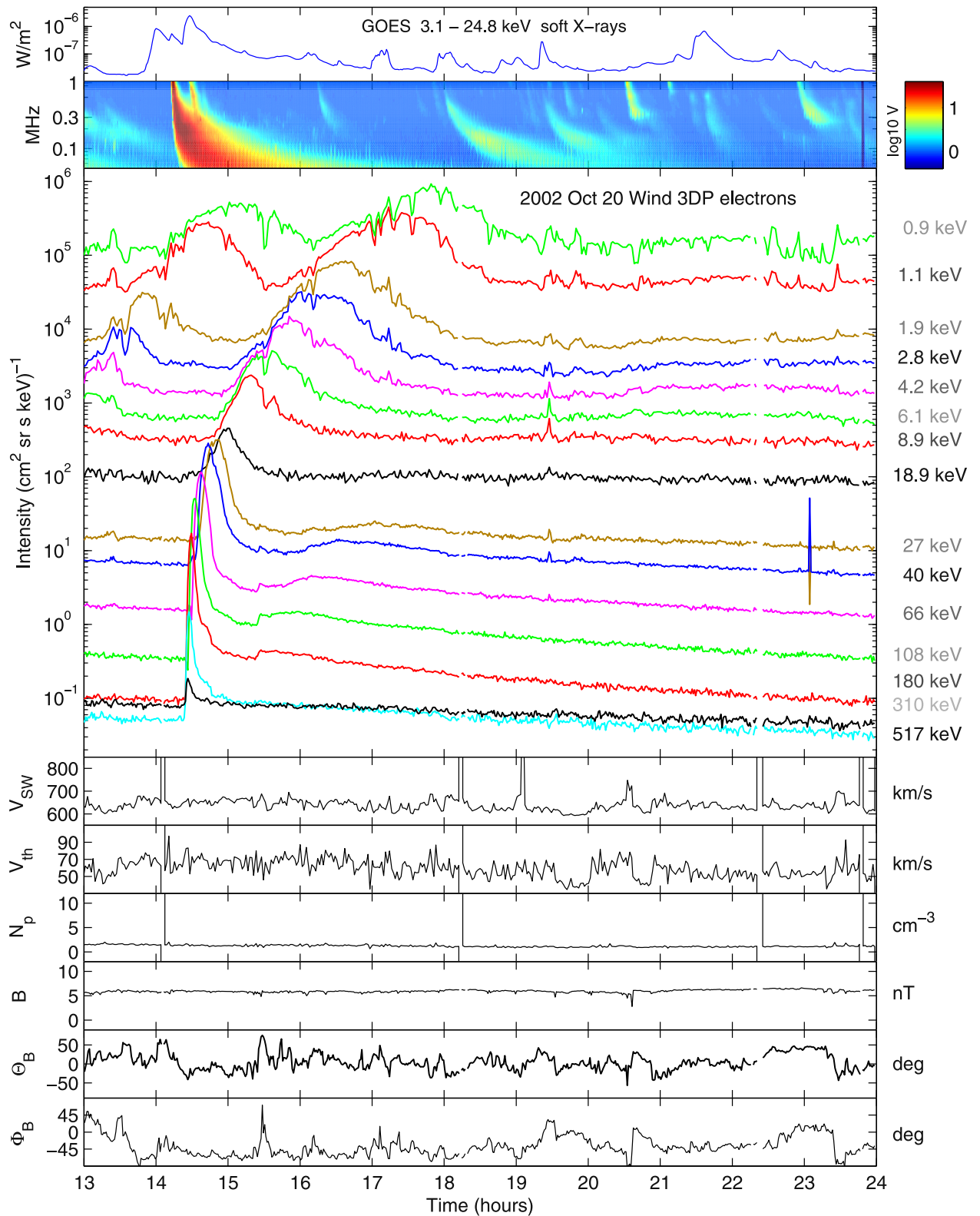


**Figure 1.** Observations of particle and solar wind plasma during the 2002 October 20 event. The third panel shows EESA-H and SST (from 1 minute cdf files, count-corrected) omnidirectional intensities. The plasma data were obtained from <http://cdaweb.gsfc.nasa.gov/>. Magnetic field data (in the GSE system) are also from 1 minute cdf files.

first impulsive peaks, the electron intensities between 180 and 27 keV, and also at 6.1 and 4.2 keV, clearly show the appearance of a second peak with progressively delayed onset

times, which is likely due to reflection at a distance from the Sun of  $\sim 2.7$  au along the connecting field line, corresponding to  $\sim 1.5$  au along the field line past the Earth.

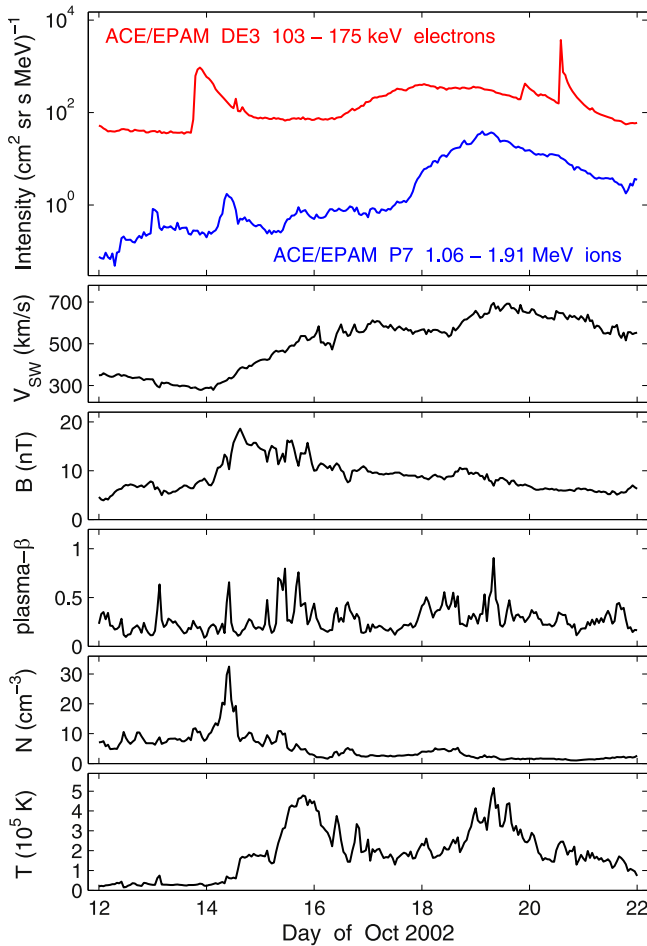


**Figure 2.** ACE particle fluxes and solar wind parameters (1 hr time resolution, downloaded from <http://cdaweb.gsfc.nasa.gov/>) during the time preceding the 2002 October 20 electron event.

In some energy channels even a third peak appears (not visible in the omnidirectional intensities shown in Figure 1, but seen in the temporal profiles of the pitch-angle distributions that will be presented in Figures 16 and following), which can be explained by the fact that the sunward-traveling electrons had been reflected a second time, now in the converging field lines close to the Sun, and are traveling outward again. The solar wind speed, shown in the fourth panel, is constantly above  $600 \text{ km s}^{-1}$ . The fifth panel shows the thermal speed, which on average adopts a value of  $\sim 60 \text{ km s}^{-1}$ . Both of the above speeds appear to exhibit considerable fluctuations on short timescales, but not on timescales of hours. On the contrary, the proton density and the magnetic field strength, shown in the sixth and seventh panels, respectively, exhibit very small fluctuations. The proton density is constantly below a very small value of  $\sim 2 \text{ cm}^{-3}$ . In turn, the elevation and azimuthal angles of the magnetic field, shown in the eighth and ninth panels, respectively, exhibit quite large fluctuations.

Figure 2 gives an overview of particle and solar wind parameters observed during a time span of 8 days before the electron event under consideration. The data seem to show no evidence for a CME and a related interplanetary shock. The solar wind speed, which had a low value of  $\sim 300 \text{ km s}^{-1}$ , starts to rise gradually after October 14 and reaches a maximum of  $\sim 650 \text{ km s}^{-1}$  on October 19. At the same time the magnetic

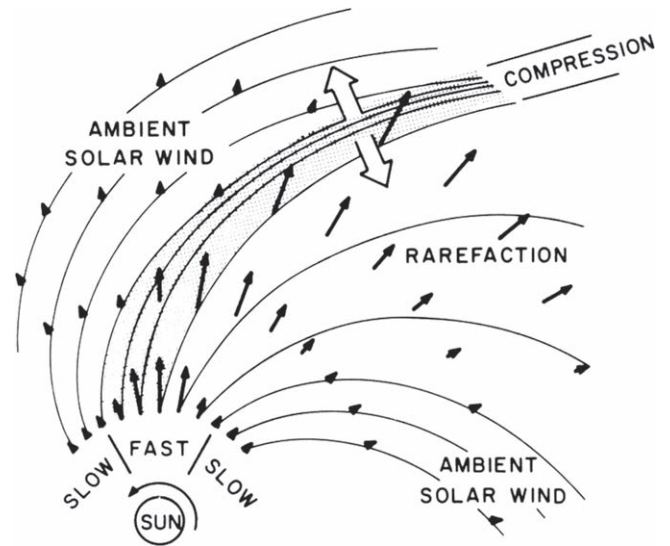


**Figure 3.** Sketch of a corotating interaction region (CIR). A compression region builds up ahead of the fast stream, while a rarefaction develops behind. Due to pressure gradients the compression region expands at the fast mode speed. A forward wave develops on the leading edge and a reverse wave on the trailing edge (reproduced from Gosling & Pizzo 1999).

field strength and the proton density drop to low values. These variations are a typical signature of the presence of a CIR, i.e., a fast solar wind stream running into a slow solar wind stream and building up a compression region at a radial distance from the Sun of  $\sim 2 \text{ au}$ , or between  $\sim 2.7$  and  $3 \text{ au}$  along the field line connecting to the Sun (e.g., Gosling & Pizzo 1999, see Figure 3). The gradual increases in low-energy electron and proton fluxes (see the upper panel of Figure 2) could be caused by particle acceleration at the CIR (Giacalone et al. 2002). We found that on <http://www.srl.caltech.edu/ACE/ASC/DATA/level3/> a pair of stream interaction regions (SIRs) is listed for 2002 October 14–15, and that the Harvard–Smithsonian Center for Astrophysics Interplanetary Shock Database (<https://www.cfa.harvard.edu/shocks/>) does not report any interplanetary shocks during 2002 October 12–20. We therefore conclude that the reflection of electrons in the 2002 October 20 event is likely due to—depending on their pitch angle—scattering or mirroring at a CIR-related compression, and not due to interaction with an interplanetary shock or propagation in a CME-related loop structure. Malandraki et al. (1997) described a technique for estimating the radial distance at which the magnetic compression arises due to stream–stream interaction by mapping the observed time variation of the solar wind speed back to the solar corona. Applying this method using the observed time profile of the solar wind speed (second panel of Figure 3), we estimate the reflectivity to be located at a radial distance of  $1.9\text{--}2.1 \text{ au}$ , corresponding to a distance along the field line connecting to the Sun of  $\sim 2.4\text{--}2.7 \text{ au}$ .

The 3DP instrument (Lin et al. 1995) on *Wind* has been operating nominally from launch to the present time, and it provides full three-dimensional measurements of electron distributions from solar wind thermal plasma to  $\sim 500 \text{ keV}$  energies. Silicon semiconductor telescopes (SSTs) measure  $\sim 25\text{--}500 \text{ keV}$  electrons with an energy resolution of  $\sim 7 \text{ keV}$  FWHM (energy channels with  $\Delta E/E = 0.3$ ), while electron electrostatic analyzers (EESA-L and EESA-H) measure  $\sim 3\text{--}30 \text{ keV}$  electrons with  $\Delta E/E = 0.2$ . The



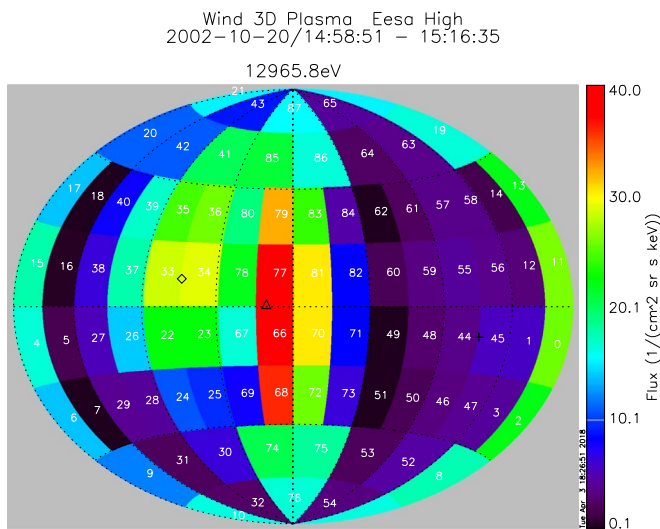


**Figure 4.** *Wind* 3DP/EESA-H three-dimensional angular distribution for  $\sim 13$  keV electron fluxes observed during the maximum phase of the 2002 October 20 electron event. Sectors are labeled by numbers, the triangle denotes the main direction of the particles, the cross (diamond) refers to the magnetic field (anti-magnetic field) direction.

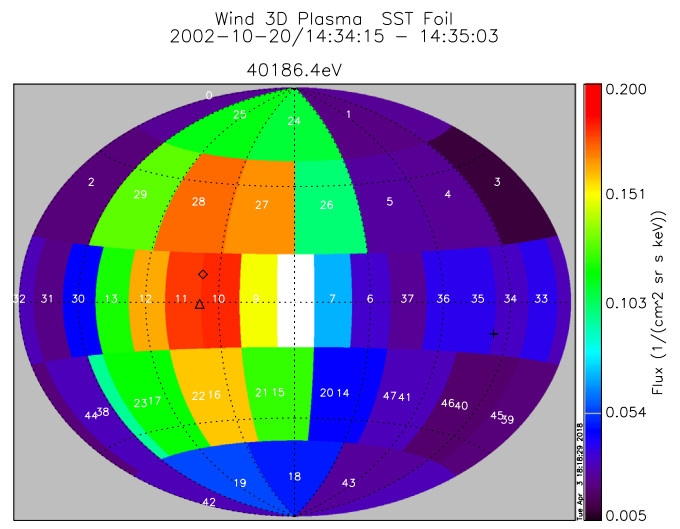


**Figure 6.** Uncorrected distribution of *Wind* 3DP/SST three-dimensional sectors (indicated by numbers) for  $\sim 40$  keV electron fluxes observed during the rising phase of the 2002 October 20 electron event. Here only the sector pointing toward the Sun has been omitted. We note that in events with larger solar X-ray fluxes more sectors might have to be excluded. Symbols have the same meaning as in Figure 4.

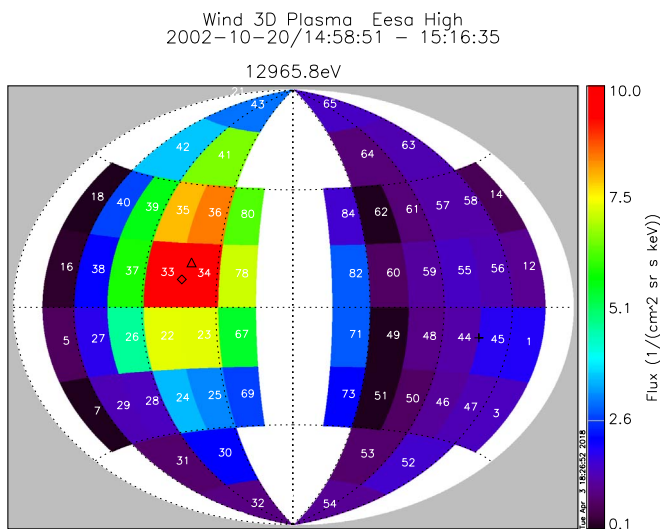


**Figure 5.** As Figure 4, but here the sectors with high background count rates due to secondary electrons caused by solar wind protons (Wang 2009, indicated by white color) have been omitted for the reconstruction of the angular distribution of the electrons. As can be seen, the direction of the magnetic field line and that of the electron streaming are now in good agreement. The indicated selection of EESA-H sectors was used to determine the angular distributions, and intensity and anisotropy profiles presented in this work.

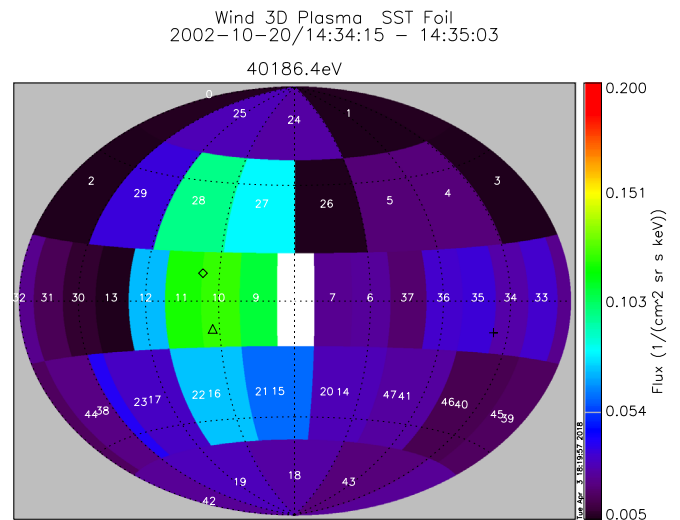


**Figure 7.** Angular distribution of  $\sim 40$  keV electrons observed by *Wind* 3DP/SST during the rise phase of the 2002 October 20 electron event after a count correction has been applied for higher energy electrons that scatter out of the detector and leave less than their incident energy. As the electrons propagate along the magnetic field, independent of their energy, the count correction does not have a strong effect on the streaming direction. Symbols have the same meaning as in Figure 4.

three-dimensional electron fluxes measured on the SST (EESA-H) are sorted on board the spacecraft into 48 (88) angular bins (Wang 2009; Tan et al. 2012), each with a roughly equal solid angle of  $22.5^\circ \times 36^\circ$  ( $22.5^\circ \times 22.5^\circ$ ). The flux in each 3D angular bin is assigned a pitch angle calculated for the center of the angular bin using the vector direction of the interplanetary magnetic field measured by the *Wind* MFI instrument (Lepping et al. 1995). Figure 4 shows an EESA-H three-dimensional angular distribution for

$\sim 13$  keV electron fluxes observed during the maximum phase of the 2002 October 20 electron event.

Besides the electron beam, which is centered around bins 33 and 34, a heavy contamination from the sunward and anti-sunward directions caused by solar wind protons is visible. The corresponding sectors (see Figure 5) are therefore omitted for the analysis. Similarly, the sector pointing toward the Sun in the SST is omitted because it is frequently distorted by solar X-rays (see Figures 6 and 7). Excluding angular bins

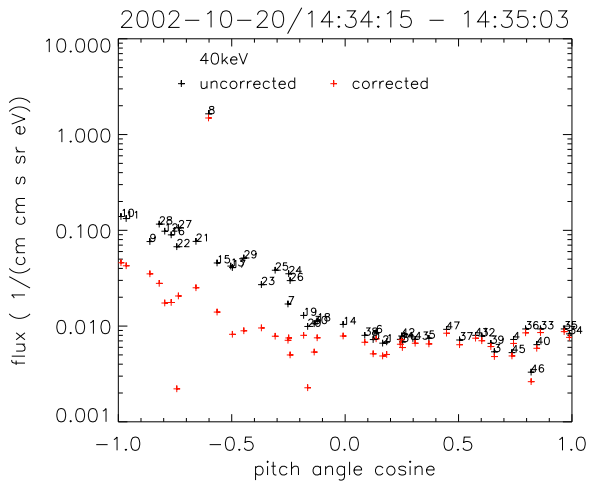


**Figure 8.** Uncorrected (black) and corrected (red) pitch-angle distributions of 40 keV electrons observed by *Wind* 3DP/SST during the rise phase of the 2002 October 20 electron event. Numbers refer to the sectors of Figures 6 and 7. Sector 8 is always distorted by solar irradiation and therefore not used in the analysis.

with high background or small geometric factors, the 3D data can then be sorted into pitch-angle bins with a resolution of  $\sim 22^\circ$ . In the SST instrument, a fraction of incident electrons scatter out of the silicon detector and deposit only a part of their incident energy in it (Wang et al. 2011; Tan et al. 2012). This part can vary as a function of the electron energy and from one solar event to another, so the original SST data downloaded from the 3DP website (<http://sprg.ssl.berkeley.edu/wind3dp/>) have not included the correction for deposition energy loss. For the 2002 October 20 event, a correction of 15%–25% is made for electrons detected in SST (Tan et al. 2012). Figure 8 compares the pitch-angle-dependent flux of 40 keV electrons before the correction (black symbols) with the one after it (red symbols). It becomes clear that without the correction the data would suggest an unphysical, too early onset of electrons in the above energy range, leading to erroneous results for their injection history and parameters characterizing their propagation. Figure 9 shows normalized EESA-H and SST pitch-angle distributions taken during the time of maximum electron intensities. The apparent widening of the distributions from  $\sim 1$  keV to hundreds of keV indicates an increase in the pitch-angle scattering as a function of energy. The agreement between the pitch-angle distributions derived from EESA-H and SST where their energy ranges overlap ( $\sim 27$  keV) is very good.

### 3. Theory

Pitch-angle scattering of SEPs is caused by fluctuations in the heliospheric magnetic field that violate the conservation of the first adiabatic invariant. When the fluctuations superposed on the average magnetic field are sufficiently small, a pitch-angle diffusion coefficient  $D_{\mu\mu}(\mu)$  can be obtained by calculating first-order corrections to the particle’s orbit in the average field, and ensemble-averaging over the statistical properties of the turbulence (Jokipii 1966). The fluctuations are considered to be small if the changes in the cosine of the particle’s pitch angle  $\mu = \cos \theta$  that they cause during a single

gyration are small and many gyrations are required to change the pitch angle significantly, implying that the particles are scattered by fluctuations that are in resonance with the particle gyration. As a cumulative result of many small random changes in its pitch angle the particle experiences a macroscopic change in its velocity component along the average field, leading to spatial diffusion along the field line. The evolution of the particle’s phase space density  $f(z, \mu, t)$  can then be described by the model of focused transport (Roelof 1969):

$$\frac{\partial f}{\partial t} + \mu v \frac{\partial f}{\partial z} + \frac{1 - \mu^2}{2L} v \frac{\partial f}{\partial \mu} - \frac{\partial}{\partial \mu} \left( D_{\mu\mu}(\mu) \frac{\partial f}{\partial \mu} \right) + \frac{f}{T_{\text{esc}}} = q(s, \mu, t). \quad (1)$$

Here  $s$  is the distance (from the center of the Sun) along the magnetic field line,  $v$  the particle speed, and  $t$  the time. The systematic forces are characterized by  $L(s) = B(s)/(-\partial B/\partial s)$ , the focusing length in the diverging magnetic field  $B$ . The transport of particles away from the flare site and their subsequent injection onto the connecting field line at some distance from the Sun are phenomenologically described by the source function  $q(z, \mu, t)$ . A possible escape of particles away from field lines connecting to the Earth due to diffusion perpendicular to the magnetic field is phenomenologically described by the escape time  $T_{\text{esc}} \sim 3L^2/(v\lambda_\perp)$ , where  $\lambda_\perp$  is the perpendicular mean free path and  $L$  denotes a characteristic length scale perpendicular to the magnetic field. This effect is probably slow, but recent modelings of solar electron events observed on multiple spacecraft (Dröge et al. 2014, 2016) have shown that perpendicular diffusion can have a measurable influence on the intensity–time profiles of the electrons. Equation (1) can be solved by numerical methods, either by finite-differences schemes (Ng & Wong 1979; Schlüter 1985) or by transforming it into the corresponding Ito stochastic differential equations (Gardiner 1983):

$$ds(t) = \mu v dt \quad (2)$$

$$d\mu(t) = \sqrt{2D_{\mu\mu}} dW_\mu(t) + \left[ \frac{v}{2L}(1 - \mu^2) + \frac{\partial D_{\mu\mu}}{\partial \mu} \right] dt \quad (3)$$

which can be solved by means of Monte Carlo simulations ( $W_\mu(t)$  denotes a Wiener process). We here employ the latter method.

The statistical properties of the irregularities ( $\delta\mathbf{B}$ ) superimposed onto the average magnetic field ( $\mathbf{B} = B_0$ ) can be characterized by their two-point, two-time correlation function. If the fluctuations are considered to be homogeneous and stationary, the correlation functions depend only on the spatial and time lags ( $R_{ij}(\zeta, \tau) = \langle \delta B_i(\mathbf{r}, t) \delta B_j(\mathbf{r} + \zeta, t + \tau) \rangle$ ) where  $\langle \rangle$  denotes the average over an ensemble of microscopic realizations of the fluctuations (e.g., Batchelor 1970). Alternatively, the fluctuations can be described by power spectra  $P_{ij}(\mathbf{k}, \omega)$ , which are obtained by taking the Fourier transforms

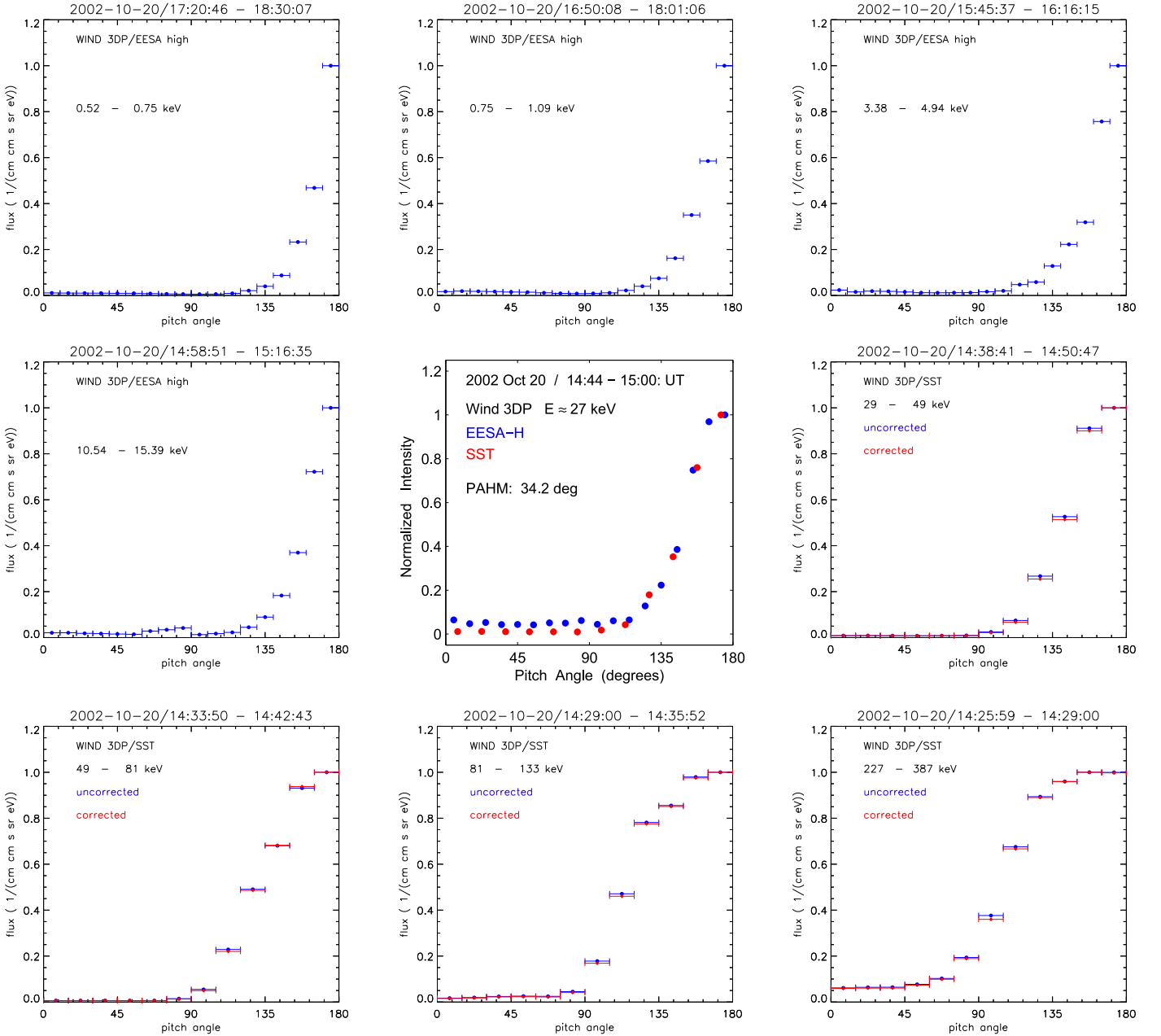


**Figure 9.** Normalized electron pitch-angle distributions in selected energy ranges observed by the *Wind* 3DP EESA-H and SST instruments at the respective times of maximum during the 2002 October 20 electron event.

of the correlation functions with respect to their spatial and time coordinates. A third possibility, which emphasizes the dynamical aspects of the correlations, is to perform the Fourier transforms only with respect to the spatial coordinates and not the time coordinate. In the following, we will consider the slab component, for which mixed spectral functions can be cast into the form (see Dröge 2003)

$$P_{ij}(\mathbf{k}, \tau) = P_{ij}(k) e^{i\omega_j^r(k)\tau - \Gamma_j(k)\tau} \delta(k_x) \delta(k_y) \quad (4)$$

where we use helical ( $i, j = R, L$ ;  $k = k_z = k_{\parallel}$ ) coordinates, which allow the spectral functions to be related to the spectral densities  $I_{R,L}^{\pm}(k)$  of forward (+) and backward (-) propagating waves with right-hand (R) or left-hand (L) polarization, and to

the helicity of the fluctuations. Here  $\omega_{R,L}^r(k)$  is the real part of the dispersion relation in the wave picture, and  $\Gamma_{R,L}(k)$  describes wave damping effects due to interactions with the warm ( $T > 0$ ) background plasma, or decorrelation effects in the turbulence picture, in which  $\omega_{R,L}^r(k) = 0$ .

The pitch-angle scattering coefficient can now be expressed as

$$D_{\mu\mu}(\mu) = \frac{\Omega^2(1 - \mu^2)}{2B_0^2} \text{Re} \int_{-\infty}^{+\infty} dk \int_0^{\infty} d\tau \times 0.5 \cdot \{ P_{RR}(k) e^{-i(k\mu\nu - \omega_R^r(k) - \Omega)\tau - \Gamma_R(k)\tau} + P_{LL}(k) e^{-i(k\mu\nu - \omega_L^r(k) + \Omega)\tau - \Gamma_L(k)\tau} \}. \quad (5)$$

Performing the integration over  $\tau$  we obtain

$$D_{\mu\mu}(\mu) = \frac{\Omega^2(1 - \mu^2)}{2B_0^2} \int_{-\infty}^{+\infty} dk \times \left\{ \frac{\Gamma_R(k)}{\Gamma_R^2(k) + (k\mu v - \omega_R^r(k) - \Omega)^2} P_{RR}(k) + \frac{\Gamma_L(k)}{\Gamma_L^2(k) + (k\mu v - \omega_L^r(k) + \Omega)^2} P_{LL}(k) \right\}. \quad (6)$$

The appearance of the function  $\Gamma(k)$  in the spectral density (4) causes a resonance broadening in the particles' interaction with the fluctuations, and the delta functions of standard QLT that describe the sharp resonance of the particles with fluctuations of a certain wavenumber are replaced by Breit–Wigner-type resonance functions (the expressions preceding the helical power spectra  $P_{RR}$  and  $P_{LL}$ , respectively, in Equation (6)). As a result, particles with a given  $\mu$  (in particular,  $\mu = 0$ ) can now be scattered by fluctuations within a finite range of wavenumbers, independent of the shape of the fluctuation spectra for  $k \rightarrow \infty$ . A number of different functional forms for  $\Gamma(k)$  have been proposed. For the turbulence picture of the fluctuations, Bieber et al. (1994) suggested a damping model with

$$\Gamma(k) = \alpha |k| V_A, \quad (7)$$

where  $V_A$  is the Alfvén speed and the parameter  $\alpha$  allows one to adjust the strength of the dynamical effects, ranging from  $\alpha = 0$  (magnetostatic limit) to  $\alpha = 1$  (strongly dynamical). The resonance functions in the pitch-angle diffusion coefficient (3) have the effect of replacing the resonance condition in the magnetostatic theory,  $k_{\text{res}} = \Omega/(\mu v)$ , by an effective resonant wavenumber

$$k_{\text{res}} \sim \frac{\Omega}{\sqrt{(\mu v \pm v_{ph})^2 + \delta^2 V_A^2}}, \quad (8)$$

which, for  $\delta > 0$  or waves propagating simultaneously parallel and antiparallel to the magnetic field with a phase speed  $v_{ph} = \omega/k$ , is always finite, indicating a non-zero scattering rate through  $90^\circ$  even for dissipation range spectra.

Observed power spectra of the fluctuations perpendicular to the average magnetic field in the inner heliosphere, e.g., of the  $z$ -component of  $\mathbf{B}$  in the GSE system, typically exhibit the following properties (e.g., Bieber et al. 1994): an energy range with a flat spectrum below wavenumbers of a few times  $10^{-7} \text{ km}^{-1}$ , followed by an inertial range with power-law exponents  $1.5 < q < 2.0$ , and a dissipation range with power-law exponents  $3 < q_d < 4$  above wavenumbers of a few times  $10^{-3} \text{ km}^{-1}$ . One possible interpretation of the fluctuations in the  $z$ -direction is that they consist partially of wave-like structures with field-aligned wavevectors (the slab component,  $\mathbf{k} \parallel \mathbf{B}$ ), and partially of structures with both  $\mathbf{k} \perp \mathbf{B}$  and  $\delta \mathbf{B} \perp \mathbf{B}$  (the 2D component). Energetic particles that propagate along  $\mathbf{B}$  would then mainly interact resonantly with the slab component and only a little or not at all with the 2D component (Matthaeus et al. 1990; Zank & Matthaeus 1992). Subsequent work (e.g., Bieber et al. 1996; Leamon et al. 1998; Dröge 2003) suggested that the slab component typically contributes 20% to the total transverse spectral power in the inertial range, and somewhat more in the dissipation range. If rotational symmetry

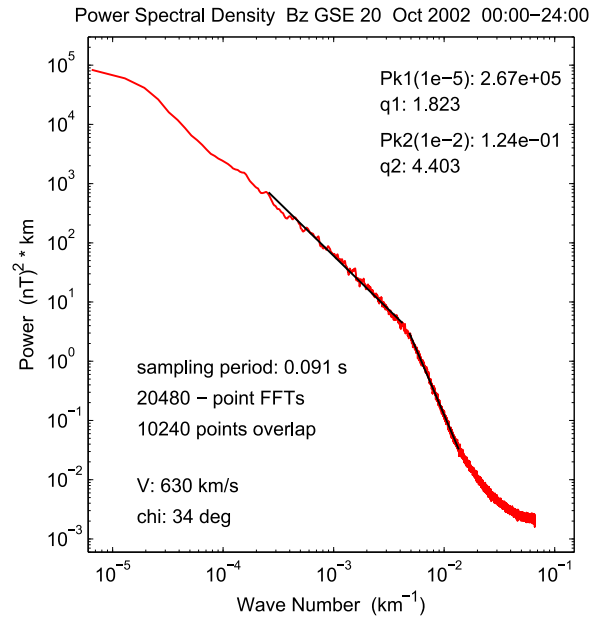


**Figure 10.** Power spectrum of the magnetic field component perpendicular to the ecliptic (in the GSE system) for the period 2002 October 20 00:00-24:00 UT.

with respect to the magnetic field direction is assumed, the GSE  $z$ -component and the component orthogonal to both GSE  $z$  and the average magnetic field direction would contribute equally to the slab component.

To proceed, we will now analyze the magnetic fluctuations observed during 2002 October 20, and investigate how much information we can obtain about the parameters that determine the pitch-angle diffusion coefficient given by Equation (6). We use *Wind*/MFI magnetic field data with a time resolution of 11 vectors/s, from which the spin tone and its harmonics were significantly reduced (NASA technical report GSFC. ABS.5528.2011). In a first step a power spectrum of  $P_{zz}(\nu)$  was computed using the following method: successive data sections were Hanning-windowed, transformed with a 20,480-point fast Fourier transform (FFT), and accumulated; linear trends were removed. The normalization is such that  $P_{zz}(\nu)$  represents the one-sided spectrum of one perpendicular component of the fluctuation, i.e.,  $\delta B_z^2 = \int_0^\infty d\nu P_{zz}(\nu)$ .

If only the slab component were present, we could reconstruct the slab spectrum in wavenumber space by noting that, due to the Doppler shift in the solar wind, fluctuations of  $B_z$  at a wavenumber  $k$  are observed at the frequency (neglecting wave propagation)

$$\nu = k V_{SW} \cos \Theta_{BV} / 2\pi \quad (9)$$

and the spectral density  $P_k(k)$ , given in the plasma frame, relates to the spectral density in frequency space in the spacecraft frame  $P_\nu(\nu)$  according to

$$P_\nu(\nu) = \frac{2\pi P_k(k)}{V_{SW} \cos \Theta_{BV}}. \quad (10)$$

The wavenumber spectrum of the  $\delta B_z$  component was calculated with standard FFT methods (Figure 10). The spectrum exhibits spectral indices of 1.8 and 4.4 in the inertial and dissipation ranges, respectively. The slab fraction of power



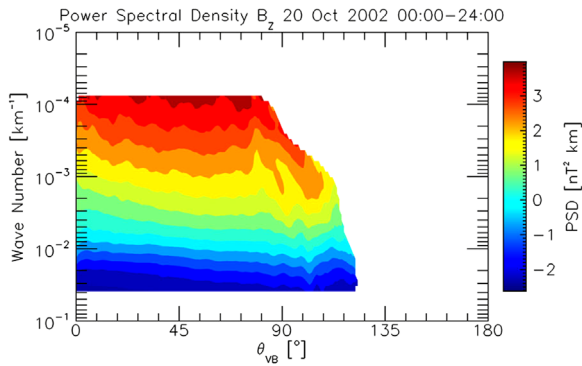


**Figure 11.** Power spectral density of the  $z$ -component of the magnetic field as a function of the angle between the orientations of the local mean magnetic field and the sampling direction.

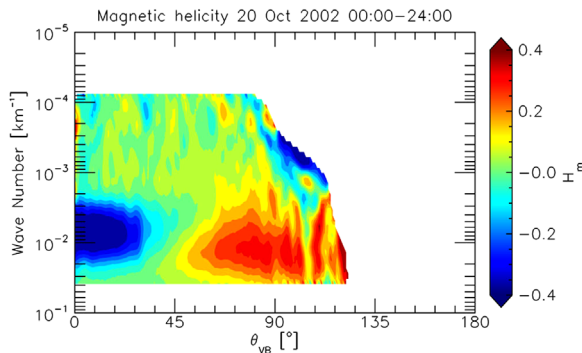


**Figure 12.** Angular distribution of the normalized magnetic helicity spectrum. The occurrence of ion cyclotron and kinetic Alfvén waves in parallel and perpendicular directions, respectively, is clearly visible.

spectral density can be estimated, e.g., by the spectral ratio method (for details see Bieber et al. 1996; Dröge 2003). Here the magnetic field data have to be transformed into a right-handed orthogonal mean-field coordinate system in which the  $z$  axis is aligned with the mean magnetic field and points away from the Sun, the  $x$  axis is in the plane defined by the mean field and the radial vector, and also points away from the Sun, and the  $y$  axis completes the right-handed system. The ratio of the power between the two transverse spectral components in frequency space would then allow an estimate of the slab fraction.

The spectral ratio method has some shortcomings, e.g., one has to assume that the transverse fluctuations consist of a slab component and a 2D component only, and that these two components have the same spectral shape over the wave-number range considered. This is why new techniques have recently been developed to investigate the slab and 2D turbulence. In particular, Horbury et al. (2008) proposed a different approach: a local mean magnetic field can be defined, at any given time and scale, as the convolution between the instantaneous magnetic field  $B_0$  and a Gaussian function (normalized to unity) whose width is the scale of interest. Fluctuations at a particular scale and at a range of angles to the local mean magnetic field can be gathered to study the solar wind turbulence in that direction. To obtain an

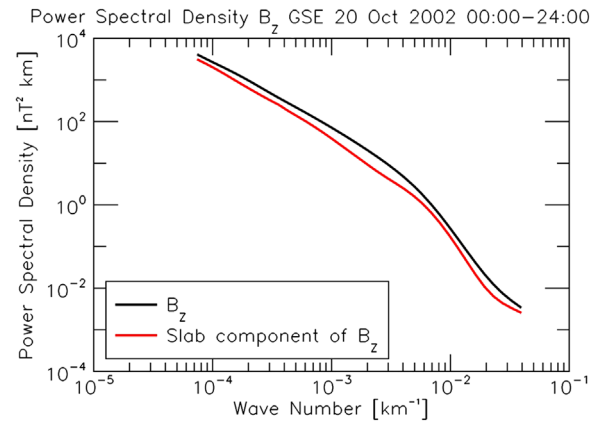


**Figure 13.** Total power of  $\delta B_z$  computed by means of the wavelet transforms (black curve) on the whole data set, and the component of the power with which the electrons interact resonantly (red curve).

estimate for the component of the turbulence that might provide the largest contribution to the scattering of the electrons, most likely fluctuations with wavevectors nearly parallel to the magnetic field (i.e., the “slab” component) with which the electrons can interact resonantly, we apply the method of wavelet transforms (e.g., Bruno & Telloni 2015). Figure 11 shows the power spectral density of the  $z$ -component of the magnetic field during 2002 October 20 as a function of the angle between the orientations of the local mean magnetic field and the sampling direction. The angular distribution of the normalized magnetic helicity spectrum of the magnetic field fluctuations is presented in Figure 12. At wavenumbers around  $k \sim 2 \times 10^{-3} \text{ km}^{-1}$  left- and right-handed polarized magnetic fluctuations, commonly associated with ion cyclotron waves and kinetic Alfvén waves, respectively (Podesta & Gary 2011; Telloni et al. 2015), are clearly resolved in quasi-perpendicular and quasi-parallel directions with respect to the local mean magnetic field. Figure 13 shows the total power spectral density,  $P_{zz}(k)$ , of the  $B_z$  component computed by means of the wavelet transforms (black curve), which is in good agreement with the spectral density determined with the standard FFT method as described above. The red curve, which makes up  $\approx 50\%$  of the transverse power, shows our estimate for the slab component. It is obtained by integrating the angular distribution of power spectral density of  $B_z$  shown in Figure 11, between  $0^\circ$  and  $10^\circ$ , i.e., over the angle range where the magnetic field vector can be considered quasi-parallel to the radial direction. In other words, the slab component is obtained by averaging, at each scale, the power spectral density found at those time instants when the magnetic field and the velocity vectors are, at that particular scale, aligned within  $10^\circ$ . It is worth noting that, since the data points involved in these averages can be very few (in an Alfvénic fast wind, such as the one considered in the present analysis, the magnetic field vector is mostly perpendicular or highly oblique to the velocity vector), the uncertainty related to the averages can be very large. As for the spectral ratio test, the underlying assumption is that  $P_{zz}(k)$  consists of two disjoint parts—a slab component with  $k_x = k_y = 0$  and a 2D component with  $k_z = 0$ —and the more the real geometry of the fluctuations deviates from the above, the larger the

uncertainty in the amount of the slab component will become. Nevertheless, the above method seems to provide the best estimate of the slab component of the solar wind fluctuations that can be provided by single-spacecraft measurements at the moment (e.g., Chen et al. 2010; Wicks et al. 2010). In the following, we adopt as a working hypothesis that a 50% slab component is responsible for the scattering of the electrons and we neglect effects of the magnetic helicity.

#### 4. Modeling

A major goal of the transport modeling in the 2002 October 20 event is the identification of the component of the turbulence that mainly determines the pitch-angle scattering of the electrons. In particular, we will investigate whether a pitch-angle diffusion coefficient calculated from the slab component within quasi-linear theory would be sufficient to explain the observed time profiles and pitch-angle distributions, or whether additional scattering due to other mechanisms (nonlinear, non-resonant effects, mirroring, interaction with the 2D component) or turbulence geometries other than the relatively simple slab/2D model would be required. To make the pitch-angle diffusion coefficient more manageable for the modeling we assume that it consists of two terms: one describing contributions from resonant interactions of the electrons with the slab component, and a second describing non-resonant scattering that might occur if electrons interact with other constituents of the turbulence, i.e., if they occasionally scatter off strong magnetic irregularities that have a scale comparable to their gyro radius, or are mirrored due to interactions with fluctuations in the magnitude of the magnetic field (Goldstein et al. 1975; Smith 1992):

$$D_{\mu\mu}(\mu) = D_{\mu\mu}^S(\mu) + D_{\mu\mu}^{NR}(\mu). \quad (11)$$

We assume that the non-resonant part of the pitch-angle diffusion coefficient leads to isotropic scattering, i.e., it is of the form  $D_0(1 - \mu^2)$ . From the considerations above—rotational symmetry around the magnetic field, small magnetic helicity, 50% slab fraction—we assume that the power spectral density relevant for resonant particle scattering is given by

$$P_{\perp}^{\text{slab}} \approx 0.5P_{\perp} \approx 0.5(P_{RR} + P_{LL}) \approx P_{zz}. \quad (12)$$

For simplicity we neglect the speed of the waves ( $\omega(k) = 0$ ) and remove the effects of the resonance broadening in Equation (6) by assuming  $\Gamma \rightarrow 0$ , which transforms the Breit–Wigner resonance functions into  $\pi \delta(kv|\mu| - \Omega)$ . Later we will reinstall the effects of resonance broadening and other effects that might scatter particles through  $\mu = 0$  by appropriate ad hoc parameters. From the total slab component derived in Section 3 (i.e., twice the slab component of  $\delta B_z$  if we assume rotational symmetry around the magnetic field) we recover the classical QLT result (e.g., Jokipii 1966)

$$D_{\mu\mu}^S(\mu) = \frac{\pi}{4} \frac{\Omega^2(1 - \mu^2)}{B_0^2 v |\mu|} P_{\perp}^{\text{slab}} \left( k_{\text{res}} = \left| \frac{\Omega}{\mu v} \right| \right). \quad (13)$$

To actually calculate the pitch-angle diffusion coefficient we parameterize the reconstructed slab component of the  $B_z$

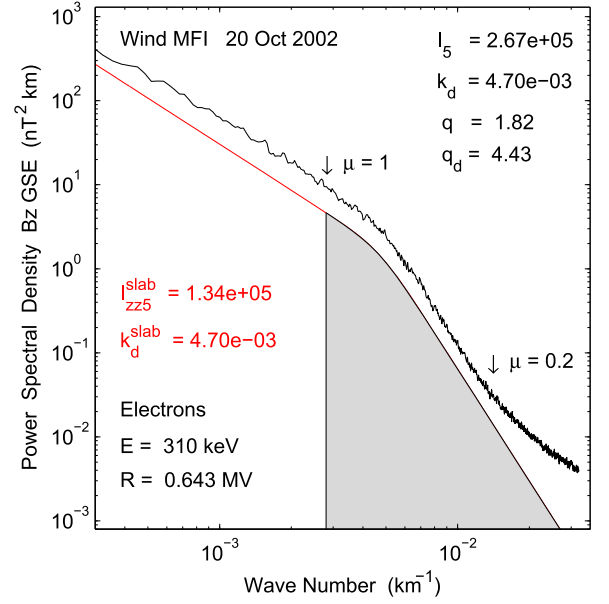


**Figure 14.** Power spectral density of  $B_z$  (black) and of the slab fraction of  $B_z$  (red). The smooth curve represents a double power-law fit to the observed spectra (assuming a slab fraction of 50%), which is used for calculating the pitch-angle diffusion coefficient. The hatched area indicates the range of wavenumbers in which 310 keV electrons interact resonantly with the fluctuations, starting at  $\sim 7 \times 10^{-3} \text{ km}^{-1}$  for a cosine of pitch angle of  $\mu = 1$ . At wavenumbers corresponding to  $\mu = 0.2$  the spectrum starts to flatten, probably due to noise in the magnetometer.

fluctuation spectrum by the functional form

$$I_{zz}^{\text{slab}}(k) = I_{zz5}^{\text{slab}} \frac{(k/k_5)^{-q}}{[1 + (k/k_d)^n]^{(q_d - q)/n}}, \quad (14)$$

where  $k_5$  is the wavenumber in units of  $10^{-5} \text{ km}^{-1}$ ,  $I_{zz5}^{\text{slab}} = I_{zz}^{\text{slab}}(k = 10^{-5} \text{ km}^{-1})$ , and  $k_d$  is the wavenumber where the dissipation range sets in. The sharpness of the transition from the power-law exponent in the inertial range to the one in the dissipation range is modeled by the parameter  $n$ . Figure 14 shows the spectral density of the  $z$ -component of the fluctuations, together with the computed slab fraction, modeled with Equation (10) for  $n = 5$ . The hatched area indicates the range of wavenumbers in which 310 keV electrons would interact resonantly with the fluctuations in magnetostatic QLT. For the parameters listed in the figure, and an observed average magnetic field strength of 6 nT, the electrons are scattered at a cosine of the pitch angle of  $|\mu| = 1$  at a wavenumber of  $\sim 3 \times 10^{-3} \text{ km}^{-1}$ . Without additional effects, there would be no scattering through  $\mu = 0$ , and the mean free path

$$\lambda_{\parallel} = \frac{3v}{8} \int_{-1}^{+1} d\mu \frac{(1 - \mu^2)^2}{D_{\mu\mu}(\mu)} \quad (15)$$

would be formally infinite. For the modeling of the time variations of the intensities, anisotropies, and pitch-angle distributions of electrons of various energies during the 2002 October 20 event we employ an ansatz for the pitch-angle

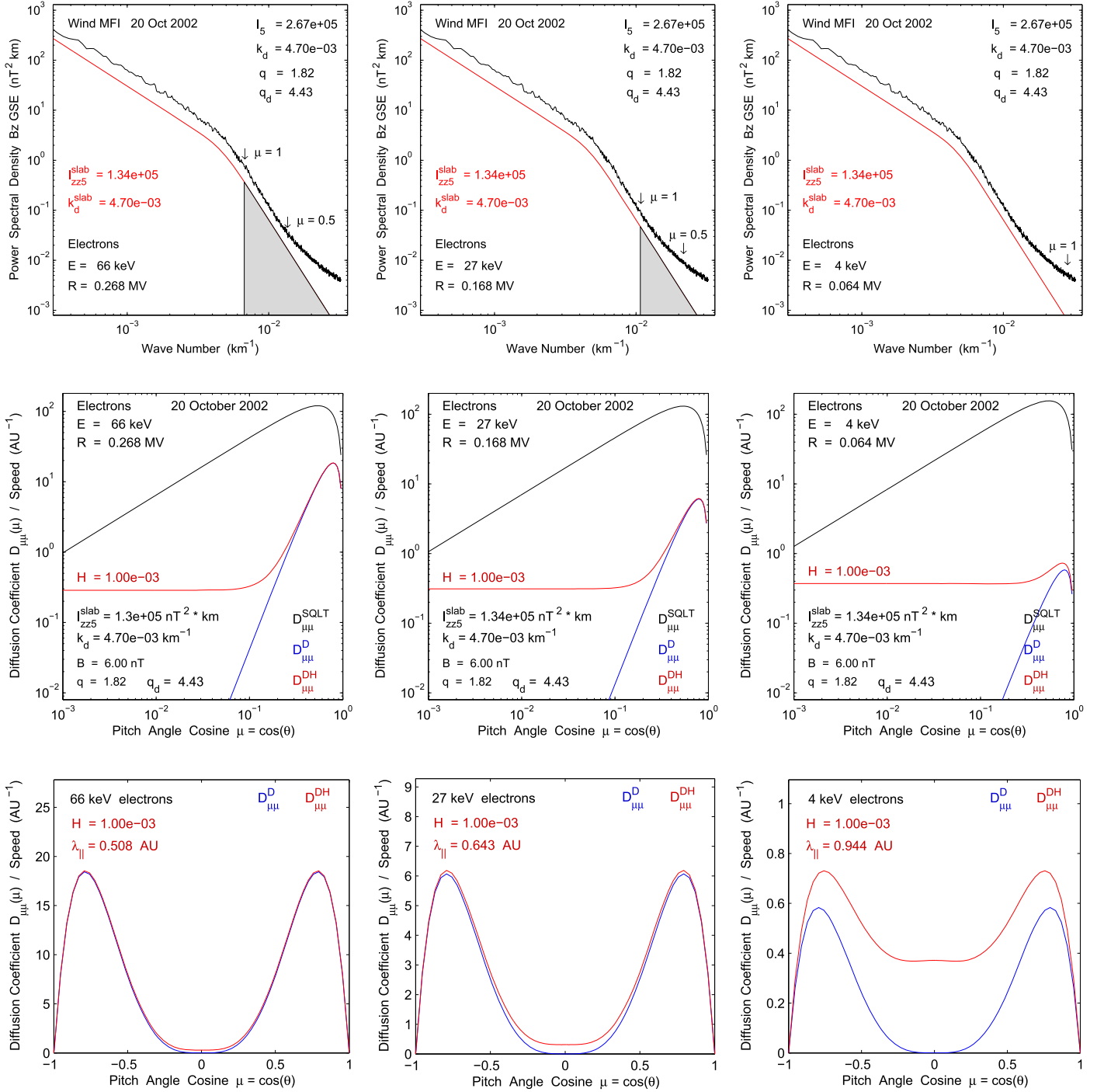


**Figure 15.** Shown here for electrons with energies of 66 keV (left row), 27 keV (middle row), and 4 keV (right row) are: power spectral density of  $B_z$  (black) and of the slab fraction of  $B_z$  (red), and the range of wavenumbers in which the electrons interact resonantly with the fluctuations in QLT (top); pitch-angle diffusion coefficient normalized to electron speed as a function of the cosine of the pitch angle for dissipationless standard QLT (black), dissipation range QLT (blue), and dynamical QLT (red) describing scattering through  $\mu = 0$  by the parameter  $H$  (middle); pitch-angle diffusion coefficients normalized to electron speed for dissipation range QLT and dynamical QLT on a linear scale (bottom).

diffusion coefficient of the form

$$D_{\mu\mu}^S(\mu) = \frac{\pi}{2} \frac{v}{R^2} (1 - \mu^2) \left( \frac{\Omega}{k_5 v} \right)^{-q} I_{zz5}^{\text{slab}} \times \left\{ \frac{|\mu|^{q-1}}{[1 + (\mu_d/\mu)^n]^{(q_d-q)/n}} + H, \right\} \quad (16)$$

where  $R$  is the rigidity of the electrons and  $\mu_d = \Omega/(k_d v)$  is the cosine of the pitch angle below which the electrons nominally interact entirely with the dissipation range of the fluctuations. The parameter  $H$ , which should not exceed unity, constitutes corrections within QLT due to resonance broadening (in which case it will be related to the parameter  $\Gamma$  in (4)), or describes nonlinear effects (e.g., Owens 1974; Völk 1975; Goldstein 1976).

To investigate whether we can relate transport parameters obtained from modelings of the observed intensity–time profiles and pitch-angle distributions (Equation (1)) of the electrons to those determined from the observed magnetic fluctuation spectra (Equations (11) and (12)) we will now consider the electron fluxes at energies of 66, 27, and 4 keV in some detail. The left, middle, and right columns of Figure 15 show in the upper row for the electrons at the above energies, respectively, the ranges of wavenumbers within which the electrons interact with the derived slab component of the fluctuations. The middle row of the figure shows calculated pitch-angle diffusion coefficients for dissipationless standard QLT, QLT taking into account the effect of the dissipation range, and dynamical QLT involving finite scattering through  $\mu = 0$  for which a value of  $H = 0.001$  had been adopted, following estimates for the effects of wave damping (Achatz et al. 1993) and of dynamical turbulence (Bieber et al. 1994; Dröge 2003). To emphasize the effect of the parameter  $H$  and for comparison with modeling results, the lower row of the figure shows the diffusion coefficients on a linear scale and also states the parallel mean free path for dynamical QLT (DQLT) calculated with Equation (15).

We note that in the 2002 October 20 event the resonant interaction for the chosen energies takes place with fluctuations that are entirely in the dissipation range. For 66 and 27 keV and at pitch angles  $\mu < 0.5$  the power spectrum at these wavenumbers is already significantly affected by the noise level of the magnetic field instrument (see Lepping et al. 1995). The figure for the 4 keV electrons shows that at this energy no predictions for the interactions of the electrons with the fluctuations can be made.

Solving Equation (1) by means of Monte Carlo simulations of the corresponding Ito stochastic differential equations (see Gardiner 1983) for the above three energy ranges, we now attempt to reproduce detailed features of the particle fluxes, in particular the time profiles of the omnidirectional intensity and the first-order anisotropy, the time profiles at selected pitch angles, and the pitch-angle distribution around the time of the maximum flux. Modeling parameters are the pitch-angle diffusion coefficient  $D_{\mu\mu}(\mu)$  and the injection function  $q(s, \mu, t)$ . We further assume that a magnetic compression is located at a distance  $s_c$  beyond 1 au at which the magnetic field strength increases from  $B_1$  to  $B_2$ , and with which the electrons interact under conservation of their first adiabatic invariant,  $\sin^2(\theta)/B = \text{constant}$ . Electrons from the sunward direction with a pitch angle  $\mu_1$  pass the compression and adopt a value of  $\mu_2^2 = 1 - (B_2/B_1)(1 - \mu_1^2)$  if  $B_1/B_2 > 1 - \mu_1^2$ , otherwise they are reflected and move toward the Sun with  $-\mu_1$ . Electrons encountering the compression from the anti-sunward direction with  $\mu_2$  always pass the compression and continue with  $\mu_1^2 = 1 - (B_1/B_2)(1 - \mu_2^2)$ . As the magnetic field is directed toward the Sun during the event (see Figure 1), anti-sunward streaming electrons with  $\theta > 125^\circ$  are transmitted. A comparison of the results of simulations with the observations for 66 keV is shown in Figures 16 and 17 respectively. The first panels of the figures indicate that the 66 keV electrons were injected  $\sim 10$  minutes after the injection of electrons with energies below 10 keV, which are mainly responsible for the emission of the type-III radio bursts (Ergun et al. 1998). The respective second to sixth panels demonstrate that the temporal

development of the observed pitch-angle distribution, intensities, and anisotropy that had been identified by Wang et al. (2011)—an initial pulse with a width of  $\sim 15$  minutes, a reflected pulse from the anti-sunward direction peaking shortly after 16:00 UT, and a faint third pulse again from an adiabatic reflection close to the Sun around 16:30—are well captured by the simulation for a location of the magnetic compression at  $s_c = 2.6$  au and a compression ratio  $B_2/B_1 = 1.5$ . The comparison of the simulation result with the pitch-angle distribution observed close to the time of maximum intensity, shown in Figure 18, exhibits an excellent agreement.

The pitch-angle diffusion coefficient (red dots in Figure 19), the distance along the magnetic field line ( $s$ ) to the magnetic compression region, and its compression ratio used for the modeling were determined by trial and error. We found that reproducing the observed intensity–time and anisotropy–time profiles would mainly depend—besides the injection profile and  $s$ —on the absolute strength of the pitch-angle scattering (parameter  $A$ ), whereas the relative timing of the intensity–time profiles at different pitch angles and the resulting time dependence of the angular distributions at 1 au would depend critically on the shape of  $D_{\mu\mu}$  (parameters  $\mu_d$  and  $H$ ). Keeping the hypothesis that the electrons interact resonantly with the slab component of the fluctuations, we have attempted to reproduce the functional form of  $D_{\mu\mu}$  from the modeling by varying the parameters describing the slab component (Equations (12), (13), and (15)). The black curve in Figure 19, which matches the pitch-angle diffusion coefficient from the modeling well, was obtained by reducing the absolute power of the slab component to  $I_{zz}^{\text{slab}} = 5 \times 10^4 \text{ nT}^2 \text{ km}$ , reducing the wavenumber where the dissipation range sets in to  $k_d = 1.46 \times 10^{-3} \text{ km}^{-1}$ , and adopting  $H = 0.0016$ . The values of the spectral indices of the turbulence spectra in the inertial and dissipation ranges were not changed.

This pitch-angle diffusion coefficient would be in strong disagreement with the one calculated from DQLT and the wavelet estimate for the slab component (see first row, bottom of Figure 15). In particular, here the slab component of  $\delta B_z$  seems to make up only approximately 20% of the total power of the  $\delta B_z$  component in the inertial range, and the spectral density turns into the dissipation range at a wavenumber that is a third of that derived from the wavelet analysis. The resulting functional form of  $D_{\mu\mu}$  is also quite different: its maximum at  $\mu \sim 0.7$  is more than a factor of 40 lower than the DQLT result, and its comparatively large value around  $\mu = 0$  indicates the presence of strong resonance-broadening, non-linear, or mirroring effects. From Equation (12) we obtain formally a diffusion mean free path  $\lambda_{\parallel} = 1.96$  au.

Figures 20–23 show the results of the modeling for the *Wind* 3DP/SST 27 keV electrons, which were obtained in a similar way to that described above. The first panels of Figures 20 and 21, respectively, suggest that the injection of the 27 keV electrons started approximately at the same time as that of the 66 keV electrons, but obviously the injection lasted significantly longer. From the pitch angle–time spectrogram in the second panel of Figure 20 we identify an initial pulse with a width of  $\sim 25$  minutes, and a reflected pulse from the anti-sunward direction peaking shortly before 17:00 UT. The slight flux enhancements around  $90^\circ$  at  $\sim 17:00$  UT and possibly also after  $\sim 17:30$  UT in the anti-sunward direction (also seen in the



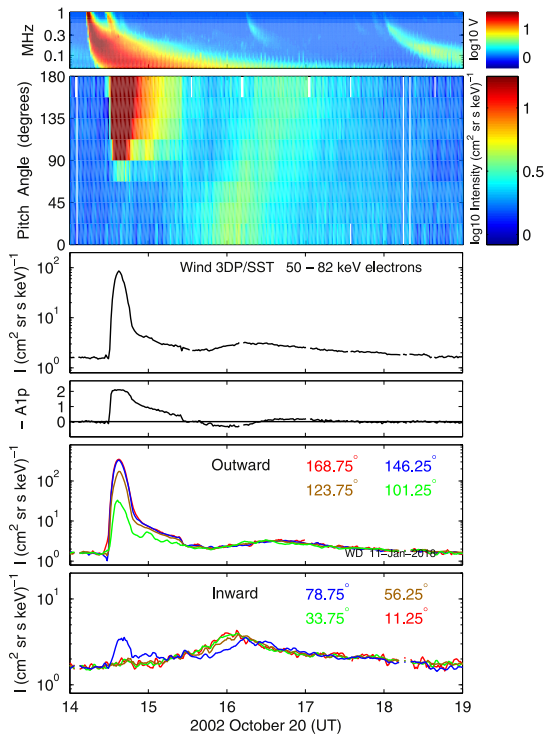


**Figure 16.** Temporal profiles of (from top to bottom) type-III radio bursts, 66 keV electron pitch-angle distribution, omnidirectional intensity, anisotropy, and fluxes for selected pitch angles in the outward and inward directions observed during the 2002 October 20 electron event.

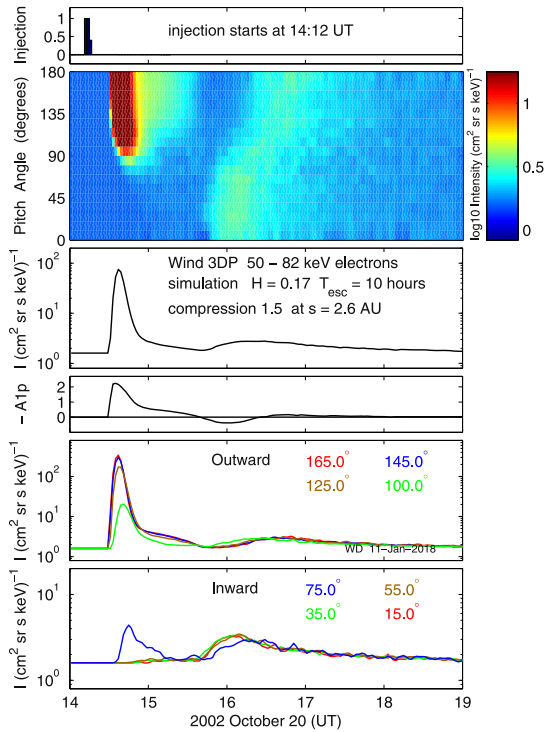


**Figure 17.** Temporal profiles of modeling results for 66 keV electrons. From top to bottom: injection function, pitch-angle distribution, omnidirectional intensity, anisotropy, and fluxes for selected pitch angles in the outward and inward directions. The pitch-angle diffusion coefficient shown in Figure 19 and particle reflection at a magnetic compression with a ratio of 1.5 located at a distance from the Sun along the magnetic field line of  $s = 2.6$  au were assumed.

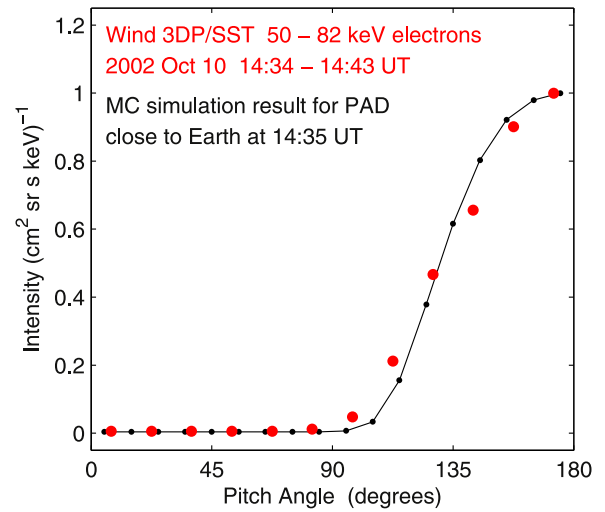


**Figure 18.** Observed pitch-angle distribution of  $\sim 66$  keV electrons in the 2002 October 20 electron event shortly before the intensity maximum (red) and the prediction of the modeling (black).

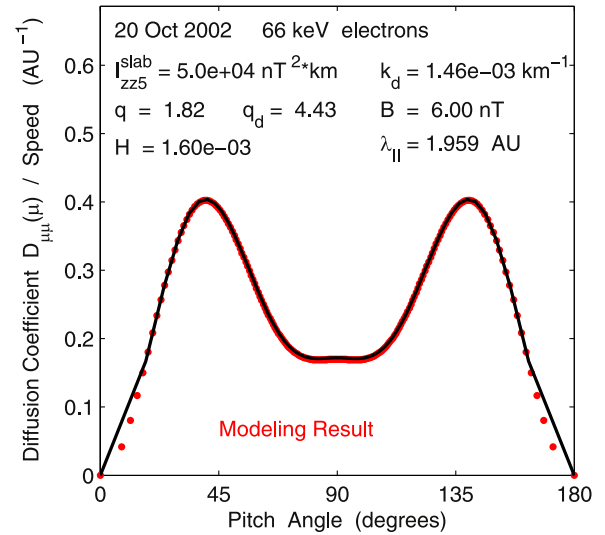


**Figure 19.** Red dots show the pitch-angle diffusion coefficient found by trial and error that provided the optimal simultaneous modeling of the observed time variations of the intensity, anisotropy, and angular distributions of  $\sim 66$  keV electrons in the 2002 October 20 electron event. The black line shows the DQLT prediction for the parameters displayed in the figure.

fifth panel), as well as the outward-pointing anisotropy (fourth panel) at that time, hint at the presence of a possible third component of 27 keV electrons reflected again close to the Sun, but we would not claim that we can unambiguously identify it from the available data. We conclude that the initial pulse with a width of  $\sim 25$  minutes and a reflected pulse from the anti-sunward direction peaking shortly after 17:30 are well reproduced by the simulation for a location of the magnetic compression at  $s = 2.6$  au and a compression ratio  $B_2/B_1 = 1.5$ . The comparison of the simulation result with the pitch-angle distribution observed close to the time of maximum intensity, shown in Figure 22, exhibits an excellent agreement. To take account of the more strongly peaked pitch-angle distribution compared to the 66 keV electrons (also visible in the outward intensity profiles, fifth panel in

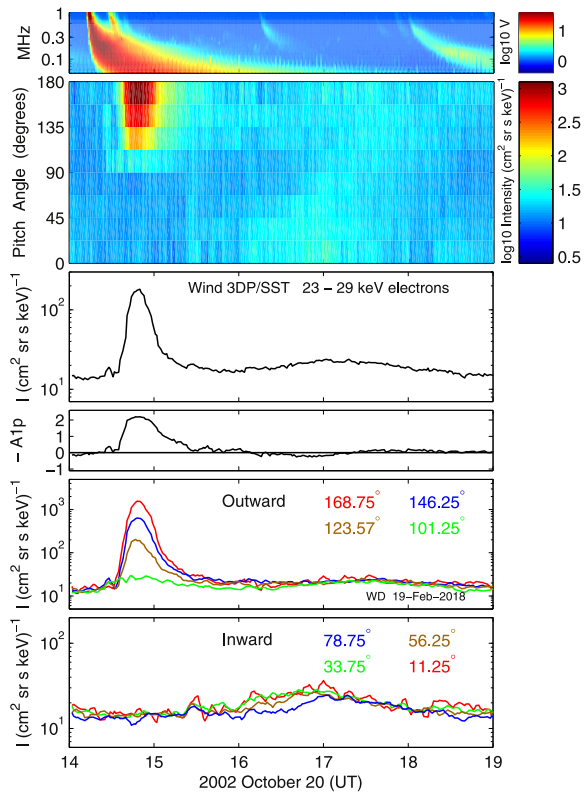


**Figure 20.** Temporal profiles of (from top to bottom) type-III radio bursts, 27 keV electron pitch-angle distribution, omnidirectional intensity, anisotropy, and fluxes for selected pitch angles in the outward and inward directions observed during the 2002 October 20 electron event.

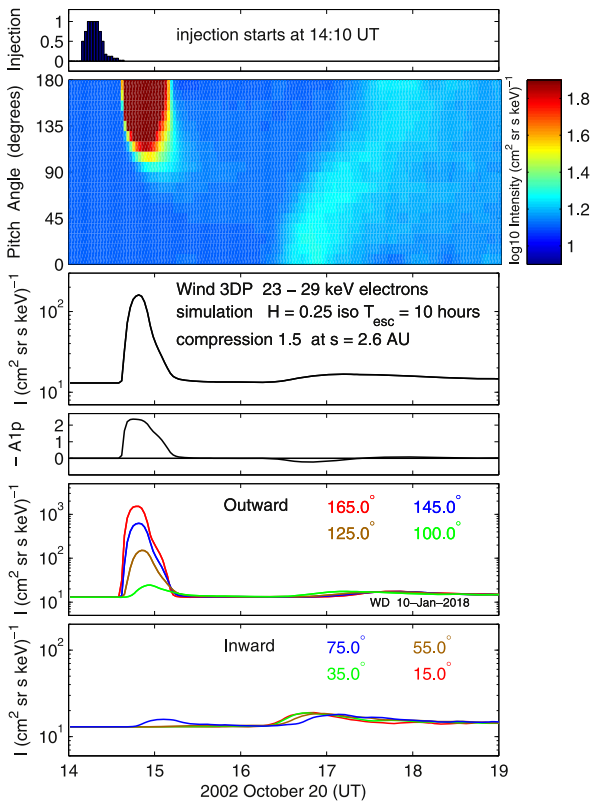


**Figure 21.** Modeling of 27 keV electron fluxes at selected pitch angles during the 2002 October 20 electron event. The pitch-angle diffusion coefficient shown in Figure 23 and particle reflection at a magnetic compression with a ratio of 1.5 located at a distance from the Sun along the magnetic field line of  $s = 2.6$  au were assumed.

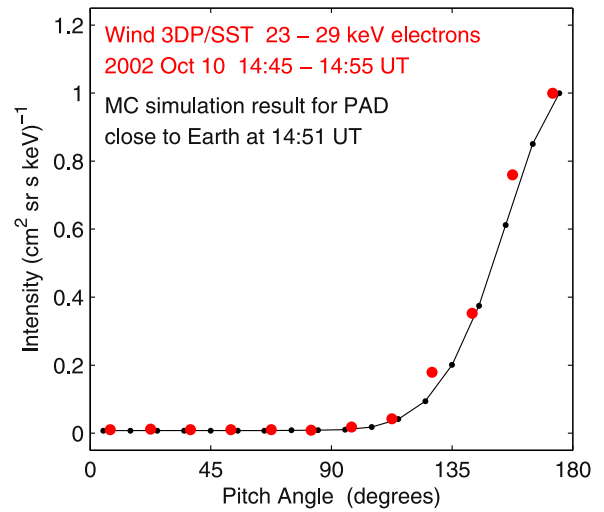


**Figure 22.** Observed pitch-angle distribution of  $\sim 27$  keV electrons in the 2002 October 20 electron event shortly before the intensity maximum (red) and the prediction of the modeling (black).

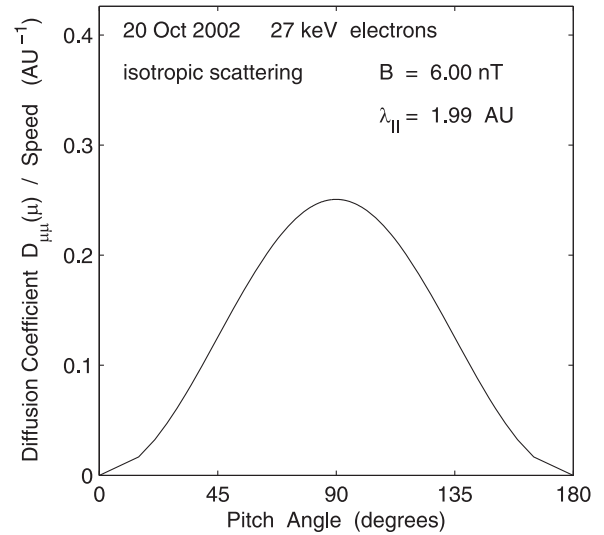


**Figure 23.** Pitch-angle diffusion coefficient found by trial and error that provided the optimal simultaneous modeling of the observed time variations of the intensity, anisotropy, and angular distributions of  $\sim 27$  keV electrons in the 2002 October 20 electron event.

Figures 20 and 21), stronger pitch-angle diffusion through  $\mu = 0$  had to be assumed. Finally, the modeling resulted in an “isotropic scattering” type of pitch-angle diffusion coefficient  $\sim (1 - \mu^2)$ , which one might expect for scattering at fluctuations with a single power-law spectral index of  $q = 1$  (see Equation (16)), although this can be excluded here, or with pitch-angle scattering due to mirroring. As for the 66 keV electrons, this pitch-angle diffusion coefficient (corresponding to a mean free path  $\lambda_{||} = 1.99$  au, see Figure 23) is in contradiction with the DQLT/slab prediction (second row, bottom of Figure 15). Our findings suggest that the 27 keV electrons do not interact resonantly with the predicted slab component but are rather scattered by a non-resonant effect such as mirroring.

We now proceed to a modeling of electrons detected by the *Wind* 3DP/EESA-H instrument. Figure 24 shows a close-up

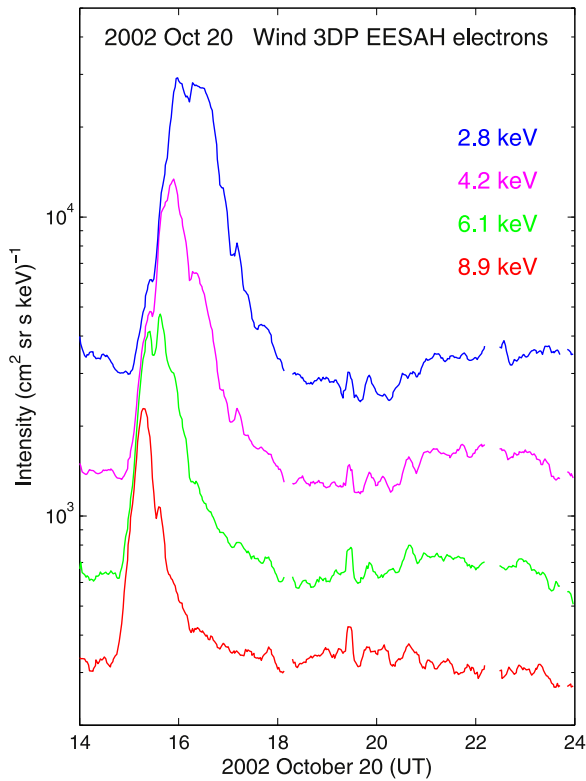


**Figure 24.** *Wind* 3DP EESA-H time-intensity profiles of the four energy ranges where a second peak is clearly visible. The shift in the onset from higher to lower energies suggests that these peaks are due to a reflection of the flare particles and not caused by local variations in the solar wind.

of omnidirectional electron fluxes in four energy channels between 2.8 and 8.9 keV. All channels clearly exhibit the prompt peak of electrons streaming away from the Sun and the second peak due to electrons reflected at the magnetic compression region beyond 1 au. A third peak due to another reflection close to the Sun as observed for the 66 keV electrons is not visible here, probably due to the higher background in the EESA-H instrument and higher fluxes of solar wind suprathermal electrons at those energies. Detailed results of the modeling of the *Wind* 3DP/EESA-H 4 keV electrons are presented in Figure 25–28. Considering that the EESA-H data are somewhat more noisy we find that, on the whole, the modeling results are in very good agreement with the observations. The derived injection profile of the 4 keV electrons, shown in the first panel of Figure 27, suggests that the injection started approximately 10 minutes earlier than that of the higher energy electrons observed by the SST instrument, but lasted much longer. Such a behavior had been reported earlier for other electron events (Wang et al. 2006, 2016). The shape of the first pulse resembles that of the injection function, indicating that electrons at 4 keV undergo considerably less pitch-angle scattering than at the energy ranges considered above. A comparison of the pitch angle-time spectrograms for the observed and simulated 4 keV electrons (second panels of Figures 25 and 26, respectively) shows that the shape of the first electron pulse is well reproduced. The predicted flux of electrons reflected by the outer boundary (for which the modeling required a

compression ratio of 2 and a location at  $s = 2.7$  au) between approximately 20:30 UT and 22:00 UT is in reasonably good agreement with observed electron fluxes with pitch angles from  $0^\circ$  to  $90^\circ$ . The fact that from  $\sim 22:00$  UT and 24:00 UT the observations seem to show an electron flux above background at pitch angles between  $45^\circ$  and  $135^\circ$  (but not before and thereafter) might indicate that some electrons were reflected close to the Sun and appeared at 1 au again. The respective third and fourth panels of Figures 25 and 26 show that the time behavior of the observed intensities and anisotropies is in very good agreement with the results of the modeling. The fifth panels of the above figures compare the observed and simulated intensity profiles of the anti-sunward streaming electrons in four ranges of pitch angle. As can be seen, the simulation results provide a very good reproduction of the observed fluxes, both of the absolute intensity values and of their temporal development. A comparison of the simulation result with the pitch-angle distribution of the 4 keV electrons observed close to the time of maximum intensity is shown in Figure 27. As can be seen, the distribution obtained from the modeling described above is distinctively wider than the observed distribution. Attempts to further reduce the absolute value of  $D_{\mu\mu}$  in the simulation resulted in somewhat narrower pitch-angle distributions, but at the cost of worsening the excellent agreement between the observed and simulated time profiles described above.

For the fine-tuning required to bring the simulated time profiles into accordance with the observed ones it was actually necessary to carefully adjust the pitch-angle dependence of the assumed  $D_{\mu\mu}$ , more so than only its absolute value. The pitch-angle diffusion coefficient found for the modeling of the 4 keV electrons, which resembles so-called “isotropic scattering” and formally would correspond to a diffusion mean free path  $\lambda_{\parallel} = 2.48$  au, is shown in Figure 28. As in the case of the higher energy electrons, this  $D_{\mu\mu}$  would be in contradiction with the DQLT/slab prediction (third row, bottom of Figure 15). We conclude that also the 4 keV electrons do not interact with the estimated slab component as predicted by QLT and an ad hoc mechanism that transports the particles through  $90^\circ$ .

To further illustrate the apparent discrepancy between the strength of the scattering predicted by theory and that derived from the modeling we show in Figure 29 again for 66 keV electrons the observed power spectrum of the  $z$ -component of the magnetic field (black), the slab component estimated from the wavelet transforms analysis (red), and the power spectrum (green) that would produce the pitch-angle diffusion coefficient used for the modeling (see Figure 19). In the range of wavenumbers in which these electrons, according to QLT, interact resonantly with the fluctuations (indicated by the gray area) the slab component would then make up only  $\sim 1\%$  of  $P_{\perp}$ . Such a low value would be an order of magnitude below typical slab fractions of 20% found for a number of solar particle events with the spectral ratio method (Bieber et al. 1994; Dröge 2003). Using spatial autocorrelation functions, Osman & Horbury (2009) presented estimates of the power in the slab and the 2D components of the turbulence from simultaneous measurements made by the four *Cluster* spacecraft when they were in the solar wind. Their results confirmed an average of 80% for the slab

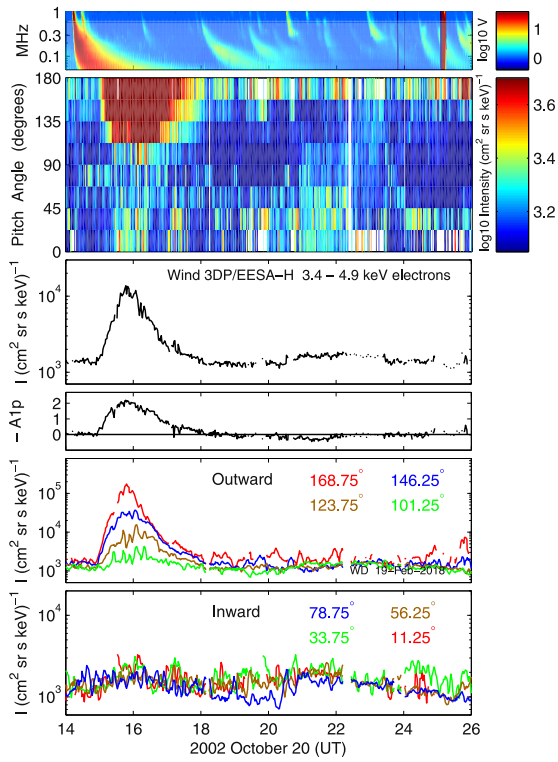


**Figure 25.** Temporal profiles of (from top to bottom) type-III radio bursts, 4 keV electron pitch-angle distribution, omnidirectional intensity, anisotropy, and fluxes for selected pitch angles in the outward and inward directions observed during the 2002 October 20 electron event.

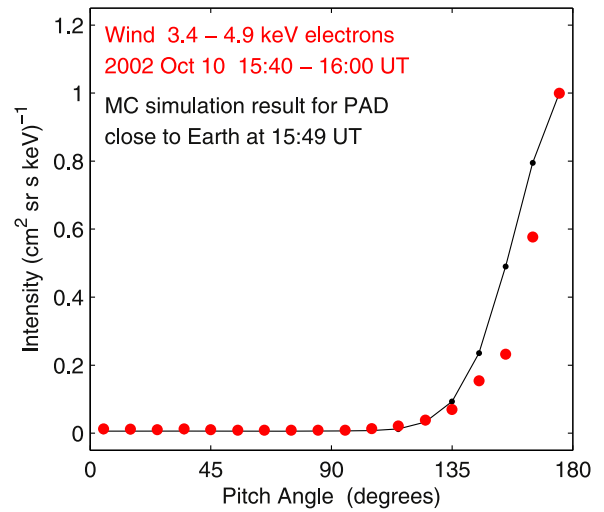


**Figure 27.** Observed pitch-angle distribution of  $\sim 4$  keV electrons in the 2002 October 20 electron event shortly before the intensity maximum (red) and the prediction of the modeling (black).

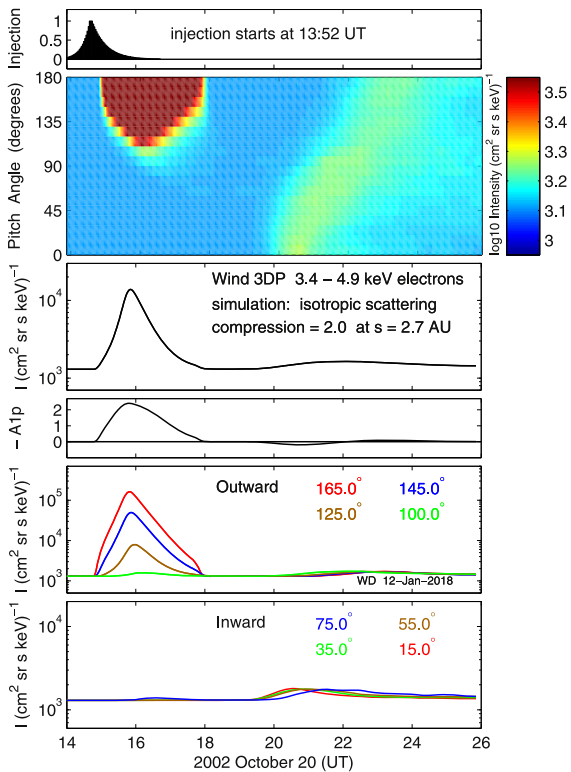


**Figure 26.** Modeling of 4 keV electron fluxes at selected pitch angles during the 2002 October 20 electron event. The pitch-angle diffusion coefficient shown in Figure 28 and particle reflection at a magnetic compression with a ratio of 2.0 located at a distance from the Sun along the magnetic field line of  $s = 2.7$  au were assumed.

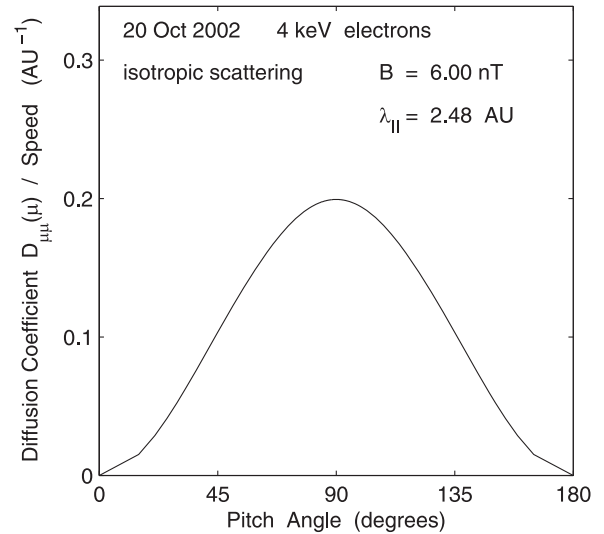


**Figure 28.** Pitch-angle diffusion coefficient found by trial and error that provided the optimal simultaneous modeling of the observed time variations of the intensity, anisotropy, and angular distributions of  $\sim 27$  keV electrons in the 2002 October 20 electron event.

component, but also time periods with values of more than 90% were identified. There is also still the possibility that the “slab+2D” hypothesis is a too highly idealized model for the decomposition of the fluctuations, and alternative distributions in wavevector space, such as the “critical balance” form suggested by Goldreich & Sridhar (1995), would have to be considered. Chen et al. (2010, their Figure 2) presented a turbulence model with critical balance in which the power in the magnetic field fluctuations varying along the local mean magnetic field (the slab component) adopts a spectral index of  $-2$  in the inertial range and  $-5$  in the dissipation range, leading to a reduced power in the dissipation range similar to that derived from the modeling of the 66 keV electrons. If one of the two latter turbulence scenarios were realized in the solar wind, the resulting scattering of electrons with energies of tens of keV would be very weak.



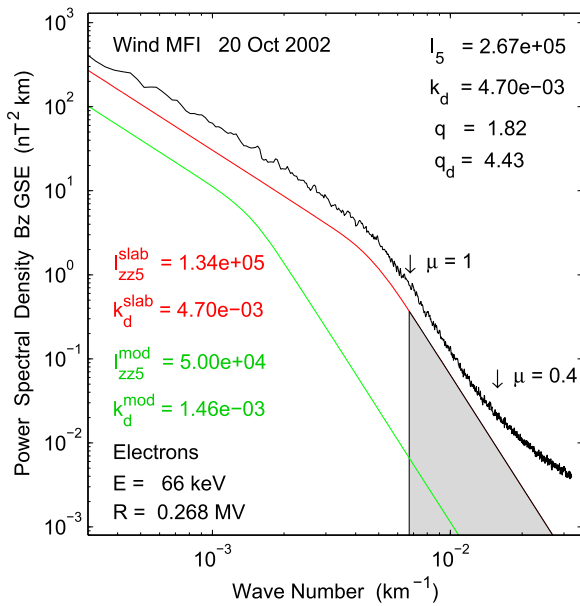


**Figure 29.** Power spectral density of  $B_z$  (black), of the estimated slab fraction of  $B_z$  (red), and of a hypothetical slab component that would produce the pitch-angle diffusion coefficient found for the modeling of the 66 keV electrons.

## 5. Discussion and Conclusions

In this work we have presented a detailed modeling of the transport of 4–66 keV electrons in the 2002 October 20 impulsive solar particle event, making use of—to our knowledge, the first time for this purpose—the full angular resolutions of the *Wind* 3DP EESA-H and SST instruments. We find that the propagation of the electrons in the interplanetary magnetic field is not really “scatter-free,” as events of this type are frequently referred to. There is weak, but finite scattering at all pitch angles, including the pitch-angle transport through  $90^\circ$ . Maybe the denotation “weak scattering” would be more appropriate for this type of event. The modeling also reproduces well the effects of particle reflection at an outer boundary, which is probably caused by a magnetic compression related to a corotating interaction region at a distance of  $\sim 2.7$  au from the Sun along the connecting field line, and subsequently again close to the Sun due to mirroring in the converging magnetic field lines. The pitch-angle diffusion coefficients obtained from the modelings are distinctly different from those calculated using the observed power spectra of the fluctuations and a slab fraction of 50% obtained by wavelet transform analysis, which is a proven method. The absolute values and the pitch-angle dependence of the derived diffusion coefficients  $D_{\mu\mu}$  would be in better agreement with those derived from a Goldreich–Sridhar turbulence model in which the power of fluctuations along the magnetic field direction falls off faster than that of fluctuations perpendicular to it, and makes up only a few per cent of the total power at large wavenumbers.

We note from Figures 19, 23, and 28 that the pitch-angle diffusion coefficients of the 66, 27, and 4 keV electrons, normalized by their respective speeds, all adopt values of  $\sim 0.2$  au $^{-1}$  at  $\mu = 0$ , indicating that  $D_{\mu\mu}$  scales with the electron speed. Furthermore, the  $\mu$ -dependence of the pitch-angle diffusion coefficients found for the 4 and 27 keV electrons clearly resembles a  $\propto(1 - \mu^2)$  “isotropic scattering” shape.

A pitch-angle diffusion coefficient that has the above properties is that for magnetic mirroring (e.g., Fisk et al. 1974; Owens 1974; Smith 1992):

$$D_{\mu\mu}^M(\mu) \approx \frac{\langle \delta B^2 \rangle}{\langle B_0^2 \rangle} (1 - \mu^2) \frac{v}{\lambda_c} \quad (17)$$

where  $B_0$  and  $\langle \delta B^2 \rangle^{1/2}$  are the mean value of the magnetic field and the standard deviation of the fluctuations in its magnitude, respectively. For the 2002 October 20 event we derive  $B_0 = 6.05$  nT and  $\langle \delta B^2 \rangle^{1/2} = 0.355$  nT. The parameter  $\lambda_c$  characterizes the correlation length of the fluctuations, which typically is of the order of  $\sim 3 \times 10^6$  km, corresponding to 0.02 au (e.g., Wicks et al. 2010). With the above values we find

$$D_{\mu\mu}^M(\mu)/v = 0.17(1 - \mu^2) \text{ au}^{-1}, \quad (18)$$

which is surprisingly close to the value derived from the modelings. The detailed analysis of the angular distributions suggests that the total pitch-angle diffusion coefficient (see Equation (11)) in this event would at low energies be dominated by mirroring, whereas above  $\sim 40$  keV the electrons would experience additional scattering due to resonant interaction with the slab component for  $|\mu| \geq 0.5$ , and mirroring, as well as nonlinear or resonance-broadening effects, would scatter the electrons through  $\mu = 0$ .

A puzzling result is that the  $\sim 50\%$  slab component derived for the 2002 October 20 event from the wavelet transforms analysis, roughly consistent with typically reported values for the slab fraction of  $\sim 20\%$ , is so much larger than the one derived from the modeling. If our analysis method is not giving an erroneous result for some reason, the question arises whether one or more of the assumptions underlying the validity of QLT might be violated in weak-scattering solar particle events. One requirement is that the gyro motion of the particle stays in resonance with the oscillation of the wave for a long enough time to lead to a macroscopic change in its pitch angle, and one might ask how long is long enough. In fact, the involvement of the time in the computation of  $D_{\mu\mu}$  is in the form of an integral over time that extends from zero to infinity (see Equation (5)) and describes, besides a resonance between the wave and the gyro motion, the effects of wave damping and decorrelation. In reality, one might expect that the upper limit would have to be large compared to the gyro period of the particle and small compared to its travel time from the source to the point of observation. Another property of the turbulence that might lead to a time dependence of the power spectral densities in Equation (5) is intermittency, i.e., a randomly distributed spatial and temporal variation of the intensity of the fluctuation responsible for particle scattering along the field lines. Intermittency is a natural characteristic of turbulence, and observations have shown (Marsch & Tu 1994; Bruno et al. 2004) that the interplanetary magnetic field can be highly intermittent. Particles propagating along the magnetic field could then traverse quiet regions almost without any scattering, and from time to time encounter structures in which they are scattered frequently or even undergo large-angle scattering. A consistent mathematical theory that would be able to incorporate characteristics of the intermittency (e.g., the p-model, Meneveau & Sreenivasan 1987) into the calculation of pitch-angle diffusion coefficients, or scattering operators in the case of large-angle scattering, seems not to have been developed yet. Results of particle orbit simulations in

intermittent magnetic fluctuations for a composite (slab+2D) geometry were presented by Alouani-Bibi & le Roux (2014). They report that, due to the effect that particles are trapped for longer time periods in patches of strong turbulence, the parallel mean free path is smaller than for uniform turbulence over a wide range of rigidities. Pucci et al. (2016) performed test particle simulations in a 3D turbulence model in which intermittency was implemented by means of the above-mentioned p-model. Contrary to the results of Alouani-Bibi & le Roux (2014), they found that an increasing level of intermittency enhances parallel transport, i.e., leading to a parallel mean free path that is larger than for uniform turbulence. Although both of the above models were applied to low-energy ( $\sim 1$  MeV) protons, neglected the dissipation range of the fluctuations and the effect of adiabatic focusing, considered the spatial rather than the pitch-angle diffusion coefficient, and are therefore not directly comparable to results of our modelings, it appears that the findings of Pucci et al. (2016) could offer an explanation for the strongly reduced scattering in electron events such as the one observed on 2002 October 20.






Transport modelings using high-resolution measurements of solar particle angular distributions from *Wind* 3DP allow us to study subtle effects of the interactions of the energetic particles with magnetic fluctuations, as well as properties of the solar wind turbulence itself. In contrast to events in which the particles undergo strong scattering and their pitch-angle distributions can be more or less completely described by a first Legendre polynomial ( $\propto \mu$ ), weak-scattering electron events offer the possibility to relate the pitch-angle dependence of  $D_{\mu\mu}$  to the observed angular distributions. In particular, our finding that the pitch-angle distribution observed for the 4 keV electrons could no longer be satisfactorily described by a classical diffusion (Fokker–Planck) equation might indicate that at low electron energies the basic assumptions of resonant quasi-linear theory are no longer fulfilled. In this context it should be noted that every solution of a Fokker–Planck equation (such as Equation (1)) implies an infinite speed of propagation—in our case in  $\mu$ -space—which could result in too fast a widening of a narrow pitch-angle distribution such as the one shown in Figure 27.

The modeling of weak-scattering events observed on a single spacecraft can, in principle, also provide some information about the transport of the electrons perpendicular to the magnetic field. For well connected events the escape time  $T_{\text{esc}} \sim 3L^2/(v\lambda_{\perp})$  describes a loss of electrons due to perpendicular diffusion from the connecting field line, which might lead to an additional small, but finite decrease of the intensity with time. Diffusion across the mean magnetic field can be caused by particles propagating along meandering field lines (field line random walk, e.g., Jokipii & Parker 1969) or by scattering of the particles at magnetic fluctuations that relocate their gyro centers between neighboring field lines. Dröge et al. (2016) used multi-spacecraft measurements to perform a three-dimensional transport modeling of a series of solar electron events observed in 2010 August. They found values for the perpendicular diffusion coefficient at 1 au of  $\lambda_{\perp} \sim 0.007$  au, which would be consistent with predictions from the field line random walk model. Dresing et al. (2014) performed a statistical survey of widely spread out solar electron events observed on *STEREO* and *ACE*, and found that the longitudinal variation of the peak intensities at 1 au could roughly be

characterized by a Gaussian distribution with a standard deviation  $\sigma$  of approximately  $40^\circ$ . We find that for the 66 and 27 keV electrons in the 2002 October 20 event the inclusion of an escape time of  $T_{\text{esc}} = 10$  hours would improve the modeling after the first peak, whereas the modeling of the 4 keV electrons would be consistent with an infinite escape time. If we assume that the above length scale  $L$  perpendicular to the magnetic field is related to the angular spread of the electrons at a radial distance 1 au according to  $L \sim 2\pi\sigma/360$  au, and that because of the apparent weak interaction of the electrons with the fluctuations perpendicular diffusion is caused by field line random walk with  $\lambda_{\perp} \sim 0.007$  au, we derive from the above considerations a longitudinal spread of the 66 and 27 keV electrons with  $\sigma$  of approximately  $17^\circ$  for the 2002 October 20 event. This is significantly narrower than for the events studied by Dresing et al. (2014), but not uncommon. Klassen et al. (2016) investigated 55–65 keV electron fluxes observed simultaneously on *STEREO-A/B* during two solar particle events on 2014 August 1, for which the respective footpoints of the magnetic field lines connecting to the two spacecraft were separated by only  $9^\circ$ . It was found that the two events observed on *STEREO-A* exhibited a pulse-shaped, anisotropic character similar to that in the 2002 October 20 event, whereas on *STEREO-B* the intensity profiles were rather diffusive and the peak intensities a factor of five lower, indicating weak perpendicular diffusion in this event. Future investigations will concentrate on more sophisticated transport modelings of electrons with energies from a few keV to a few tens of keV in weak-scattering events, which might require the diffusion term in Equation (1) to be replaced by a more general approach such as a Boltzmann collision integral (e.g., Kota 1994; Fedorov et al. 1995), and three-dimensional transport modelings of multi-spacecraft electron events in which the electron fluxes exhibit weak-scattering characteristics on at least one spacecraft.

We would like to thank the NASA National Space Science Data Center (NSSDC) and Space Physics Data Facility (SPDF) for making available the data sets used in this study. We thank the referee for helpful suggestions.

## ORCID iDs

W. Dröge  <https://orcid.org/0000-0001-8362-2259>  
 Y. Y. Kartavykh  <https://orcid.org/0000-0002-0623-6992>  
 L. Wang  <https://orcid.org/0000-0001-7309-4325>  
 D. Telloni  <https://orcid.org/0000-0002-6710-8142>  
 R. Bruno  <https://orcid.org/0000-0002-2152-0115>

## References

- Achatz, U., Dröge, W., Schlickeiser, R., & Wibberenz, G. 1993, *JGR*, **98**, 13261  
 Alouani-Bibi, F., & le Roux, J. A. 2014, *ApJ*, **781**, 93  
 Anderson, K. A., Sommers, J., Lin, R. P., et al. 1995, *JGR*, **100**, 3  
 Batchelor, G. K. 1970, *Theory of Homogenous Turbulence* (Cambridge: Cambridge Univ. Press)  
 Bieber, J. W., Matthaeus, W. H., Smith, C. W., et al. 1994, *ApJ*, **420**, 294  
 Bieber, J. W., Wanner, W., & Matthaeus, W. M. 1996, *JGR*, **101**, 2511  
 Bruno, R., Carbone, V., Primavera, L., et al. 2004, *AnGeo*, **22**, 3751  
 Bruno, R., & Telloni, D. 2015, *ApJ*, **811**, L17  
 Chen, C. H. K., Wicks, R. T., Horbury, T. S., & Schekochihin, A. A. 2010, *ApJL*, **711**, L79  
 Dresing, N., Gómez-Herrero, R., Heber, B., et al. 2014, *A&A*, **567**, A27  
 Dröge, W. 2003, *ApJ*, **589**, 1027

- Dröge, W., & Kartavykh, Y. 2009, *ApJ*, 693, 69
- Dröge, W., Kartavykh, Y., Dresing, N., Heber, B., & Klassen, A. 2014, *JGR*, 119, 6074
- Dröge, W., Kartavykh, Y., Dresing, N., & Klassen, A. 2016, *ApJ*, 826, 134
- Drury, L. O. 'C. 1983, *RPPh*, 46, 973
- Ergun, R. E., Larson, D., Lin, R. P., et al. 1998, *ApJ*, 503, 435
- Fedorov, Y. I., Shakhov, B. A., & Stehlik, M. 1995, *A&A*, 302, 623
- Fisk, L. A., Goldstein, M. L., Klimas, A. J., & Sandri, G. 1974, *ApJ*, 190, 417
- Gardiner, C. W. 1983, *Handbook of Stochastic Methods* (Berlin: Springer)
- Giacalone, J., Jokipii, J. R., & Kota, J. 2002, *ApJ*, 573, 845
- Goldreich, P., & Sridhar, S. 1995, *ApJ*, 438, 763
- Goldstein, M. L. 1976, *ApJ*, 204, 900
- Goldstein, M. L., Klimas, A. J., & Sandri, G. 1975, *ApJ*, 195, 787
- Gosling, J. T., & Pizzo, V. J. 1999, *SSRv*, 89, 21
- Haggerty, D. K., & Roelof, E. C. 2002, *ApJ*, 579, 841
- Ho, G. C., Roelof, E. C., Mason, G. M., Lario, D., & Mazur, J. E. 2003, *AdSpR*, 32, 2679
- Horbury, T. S., Forman, M., & Oughton, S. 2008, *PhRvL*, 101, 175005
- Jokipii, J. R. 1966, *ApJ*, 146, 480
- Jokipii, J. R., & Parker, E. N. 1969, *ApJ*, 155, 777
- Klassen, A., Dresing, N., Gómez-Herrero, R., Heber, B., & Müller-Mellin, R. 2016, *A&A*, 593, A31
- Kota, J. 1994, *ApJ*, 424, 1035
- Krucker, S., Larson, D. E., Lin, R. P., & Thompson, B. J. 1999, *ApJ*, 519, 864
- Leamon, R. J., Smith, C. W., Ness, N. F., & Matthaeus, W. H. 1998, *JGR*, 103, 4775
- Lepping, R. P., Acuña, M. H., Burlaga, L. F., et al. 1995, *SSRv*, 71, 207
- Lin, R. P. 1974, *SSRv*, 16, 189
- Lin, R. P., Anderson, K. A., Ashford, S., et al. 1995, *SSRv*, 71, 125
- Malandraki, O. E., Kasotakis, G., Sarris, E. T., et al. 2002, *JASTP*, 64, 517
- Malandraki, O. E., Sarris, E. T., Lanzerotti, L. J., Trochoutsos, P., & Tsiropoula, G. 1997, *ICRC*, 1, 281
- Marsch, E., & Tu, C.-Y. 1994, *AnGeo*, 12, 1127
- Mason, G. M. 2007, *SSRv*, 130, 231
- Matthaeus, W. H., Goldstein, M. L., & Roberts, D. A. 1990, *JGR*, 95, 20673
- Meneveau, C., & Sreenivasan, K. 1987, *PhRvL*, 59, 1424
- Ng, C. K., & Wong, K. Y. 1979, *Proc. ICRC*, 5, (Kyoto), 252
- Ogilvie, K. W., Chornay, D. J., Fritzenreiter, R. J., et al. 1995, *SSRv*, 71, 55
- Osman, K. T., & Horbury, T. S. 2009, *JGR*, 114, A06103
- Owens, A. J. 1974, *ApJ*, 191, 235
- Podesta, J. J., & Gary, S. P. 2011, *ApJ*, 734, 15
- Pucci, F., Malara, F., Perri, S., et al. 2016, *MNRAS*, 459, 3395
- Qin, G., Zhang, M., Dwyer, J. R., Rassoul, H. K., & Mason, G. M. 2005, *ApJ*, 627, 562
- Reames, D. V. 1999, *SSRv*, 90, 413
- Reames, D. V., von Rosenvinge, T. T., & Lin, R. P. 1985, *ApJ*, 292, 716
- Roelof, E. C. 1969, in *Lectures in High-Energy Astrophysics*, ed. H. Ögelmann & J. R. Wayland (Washington, DC: NASA), 111
- Saiz, A., Ruffolo, D., Bieber, P., Evenson, P., & Pyle, R. 2008, *ApJ*, 672, 650
- Schlüter, W. 1985, PhD Thesis, University of Kiel
- Smith, C. W. 1992, in *AIP Conf. Proc. 264, Particle Acceleration in Cosmic Plasmas*, ed. G. Zank & T. Gaisser (New York, NY: AIP), 79
- Tan, L. C., Malandraki, O. E., Reames, D. V., et al. 2012, *ApJ*, 750, 146
- Tan, L. C., Reames, D. V., Ng, C. K., Saloniemi, O., & Wang, L. 2009, *ApJ*, 701, 1753
- Telloni, D., Bruno, R., & Trenchi, L. 2015, *ApJ*, 805, 46
- Torsti, J., Riihonen, E., & Kocharov, L. 2004, *ApJ*, 600, L83
- Völk, H. J. 1975, *RvGSP*, 13, 547
- Wang, L. 2009, PhD Thesis, University of California
- Wang, L., Krucker, S., Mason, G. M., Lin, R. P., & Li, G. 2016, *A&A*, 585, A119
- Wang, L., Lin, R. P., & Krucker, S. 2011, *ApJ*, 727, 121
- Wang, L., Lin, R. P., Krucker, S., & Gosling, J. T. 2006, *GeoRL*, 33, L03106
- Wang, L., Lin, R. P., Krucker, S., & Mason, G. M. 2012, *ApJ*, 759, 69
- Wicks, R. T., Owens, M. J., & Horbury, T. S. 2010, *SoPh*, 262, 191
- Zank, G. P., & Matthaeus, W. M. 1992, *JGR*, 97, 17189